Geophys. J. Int. (1997) **129,** 41–74

New limits on the motion between India and Australia since chron 5 (11 Ma) and implications for lithospheric deformation in the equatorial Indian Ocean

Jean-Yves Royer,[1] Richard G. Gordon,[2] Charles DeMets[3] and Peter R. Vogt[4]

[1] *Géosciences Azur* BP48-06235 *Villefranche sur mer cedex, France. E-mail: royer@ccrv.obs-vlfr.fr*
[2] *Department of Geology and Geophysics*—MS 126, *Rice University, Houston, Texas* 77005, *USA*
[3] *Department of Geology and Geophysics, University of Wisconsin, Madison, Wisconsin* 53706, *USA*
[4] *Code* 7420, *Naval Research Laboratory,* 4555 *Overlook Ave., SW Washington,* DC 20375-5320, *USA*

Accepted 1996 November 14. Received 1996 November 12; in original form 1996 May 15

SUMMARY

We present new aeromagnetic data from a 1990 survey across the Central Indian and Carlsberg ridges between 18°S and 5°N. The 86 new crossings of anomaly 5 fill a gap of more than 2000 km in previously identified crossings. We furthermore present 15 crossings from Project Magnet aeromagnetic data and 79 crossings from shipboard data to add to 56 previously identified crossings used in prior plate reconstruction work. These combine to give a total of 236 crossings of anomaly 5 flanking the Carlsberg Ridge and Central Indian Ridge. Fracture-zone crossings are extracted from satellite-derived gravity profiles from the Seasat, Geosat/ERM, ERS1 and Topex spacecraft-based altimeters giving 177 useful new crossings near anomaly 5 on 22 conjugate palaeotransform fault pairs; these data replace the 23 crossings used in prior plate reconstruction work.

These and many other new altimetry crossings along other portions of the fracture zones permit all the fracture zones flanking the Central Indian and Carlsberg ridges to be recognized and delineated. We use these new plate-motion data to improve the reconstruction of the relative positions of the African, Indian and Australian plates at chron 5 (11 Ma). The improved quality and increased number of magnetic anomaly and fracture-zone crossings allow a great shrinking relative to prior work of the uncertainties in the relative rotations since chron 5 of the African, Australian and Indian plates. The volume of the 95 per cent confidence region is 98 times smaller than found before for the Africa–India rotation, 76 times smaller than found before for the Africa–Australia rotation, and 188 times smaller than found before for the Australia–India rotation. Unlike prior work, in which the Africa–Australia rotation depended strongly on estimates of Australia–Antarctica and Africa–Antarctica rotations, the Africa–Australia rotation can now be estimated accurately from data only along the Central Indian Ridge. The new small-confidence regions exclude all prior best estimates of these rotations. The much smaller uncertainties on the Australia–India rotation lead to specific predictions about where north–south divergence has been occurring, where north–south convergence has been occurring, and where the spatial integral of deformation is small.

As has recently been shown to be true also for plate motion since chron 2A (3 Ma), the predictions are consistent with independent observations of the location, geographical limits, and style of deformation in the diffuse plate boundary between India and Australia. In particular, the pole of rotation lies in an apparently non-deforming region between the western diffuse plate boundary characterized by north–south stretching and the eastern diffuse plate boundary characterized by north–south to northwest–southeast shortening. The pole of rotation of the Australian plate relative to the Indian plate has moved insignificantly during the past 11 Myr, which suggests that information from the displacements and deformation at present, since 3 Ma, and

since 11 Ma can be combined to obtain a more comprehensive kinematic model of how the relative motion between the Indian and Australian plates is and has been accommodated in the wide plate boundary. The 3 Myr average rotation of India relative to Africa is similar to that over 11 Myr, whereas the 3 Myr average rotation of Australia relative to Africa is insignificantly faster and indicates that Australia has changed to a slightly but significantly more eastward direction of motion than that over the past 11 Myr.

We also present a new statistical test for determining whether a segment of plate-motion data reflects motion between a pair of rigid plates for which relative motion can be estimated independently from other plate-motion data assumed to lie along the same plate boundary. Application of this new test to the new data demonstrates that the boundary between the Indian and Australian plate along the Central Indian Ridge must have been (and presumably continues to be) at least several hundred kilometres in north–south extent and therefore is not a typical narrow oceanic plate boundary. The rigid Australian plate continues no farther north than an unnamed fracture zone that is immediately south of the Vema fracture zone and intersects the Central Indian Ridge near 10°S. The rigid Indian plate continues no farther south than just north of an unnamed fracture zone that is just south of the Vityaz fracture zone and intersects the Central Indian Ridge near 7°S. Near the Central Indian Ridge, along a meridian at 70°E, the diffuse plate boundary has accommodated 20 ± 4 km (1-D 95 per cent confidence limits) of north–south divergence since 11 Ma (chron 5). East of the pole of rotation, in the Central Indian Basin, the net north–south convergence along meridians at 80°E and 90°E is 31 ± 7 km and 80 ± 12 km (1-D 95 per cent confidence limits), respectively. The indicated convergence along 78.8°E is significantly larger, and that along 81.5°E and 84.5°E is insignificantly larger than estimated from prior analyses of long north–south seismic profiles. The discrepancy has several possible explanations, including flattening of thrust faults with depth, motions out of the vertical plane of the seismic profile, and initiation of motion before 7.5–8.0 Ma, which is the age of initiation of deformation estimated from seismic profiles and deep-sea drilling.

Key words: Indian Ocean, lithospheric deformation, plate tectonics.

INTRODUCTION

The equatorial Indian Ocean is the outstanding example of deformation of oceanic lithosphere. The deforming region exceeds an area of 1000 km by 1000 km, and is comparable in size with many continental plate boundaries. Evidence for deformation of seafloor in the equatorial Indian Ocean has been recognized since the early 1970s, and further evidence of this deformation has been mounting since (Sykes 1970; Curray & Moore 1971; Eittreim & Ewing 1972; Moore *et al.* 1974; Stein & Okal 1978; Minster & Jordan 1978; Weissel, Anderson & Geller 1980; Curray & Munasinghe 1989). Newer seismic profiles show that the acoustic basement and overlying sediments are folded in long-wavelength undulations (Bull 1990; Bull & Scrutton 1990, 1992; Chamot-Rooke *et al.* 1993; Jestin 1994; Van Orman *et al.* 1995), as is also reflected in the undulations in gravity inferred from satellite altimetry data (McAdoo & Sandwell 1985). Thrust faults have been observed throughout a large region of the Bengal Fan, are typically spaced about every 7 km on north–south profiles, and are in many places observed to cut the oceanic crust (Bull 1990; Bull & Scrutton 1990, 1992; Chamot-Rooke *et al.* 1993; Jestin 1994; Van Orman *et al.* 1995).

More than a decade ago, Wiens *et al.* (1985) proposed that this zone of deformation be interpreted not as one of intraplate deformation of an Indo–Australian plate but as a diffuse boundary separating two plates. Later investigations of Indian Ocean plate motions have shown that the interpretation of this deforming zone as a diffuse plate boundary is useful (DeMets, Gordon & Argus 1988; DeMets, Gordon & Vogt 1994a; Gordon & DeMets 1989; Gordon, DeMets & Argus 1990; Royer & Chang 1991; Van Orman *et al.* 1995). These later investigations have also shown that several details of the original results and the interpretation of Wiens *et al.* (1985) were wrong. For example, Wiens *et al.* (1985) proposed that Arabia and India were part of a single Indo–Arabian plate, but Gordon & DeMets (1989) and Royer & Chang (1991) respectively showed that they are and have been in slow relative motion along a boundary that includes the Owen fracture zone. Thus, the diffuse plate boundary is now interpreted as separating an Indian plate from an Australian plate. Wiens *et al.* (1985) estimated that the pole of rotation between 'Indo–Arabia' and Australia is located west of the Chagos–Laccadive Ridge, implying that nearly the entire diffuse plate boundary was accommodating north–south convergence. Later work shows, however, that the pole lies near, but east, of the Chagos–Laccadive Ridge and that the western part of the diffuse plate boundary between India and Australia accommodates north–south divergence (Gordon *et al.* 1990; DeMets *et al.* 1994a). This result leads to a powerful qualitative test of the assumption of rigid Indian, Australian and African plates. It predicts that the integral of deformation rate along north–

south profiles near the eastern edge of the Chagos–Laccadive Ridge is negligible and that such integrals give increasingly large net convergence eastwards from a point near 3°S along the eastern edge of the Chagos–Laccadive Ridge and increasingly large net divergence westwards from the same point. There is in fact no evidence for current deformation near this point (Levchenko & Ostrovsky 1992), and considerable evidence for both north–south to northwest–southeast shortening in a huge zone east of this point and for north–south stretching southwest and west of this point.

Wiens *et al.* (1985) found significant non-closure of the Africa–Antarctica–Australia plate-motion circuit with a misfit of about 10 mm yr^{-1}. Later work indicated only an insignificant misfit (DeMets *et al.* 1988; Royer & Chang 1991), with an upper bound on misfit of 4–7 mm yr^{-1} (DeMets *et al.* 1994a). Molnar, Pardo-Casas & Stock (1988) found difficulty in simultaneously fitting anomaly 5 and other anomalies flanking the Carlsberg, Central Indian, and Southeast Indian ridges if they assumed that there had been a single rigid Indo–Australian plate. Royer & Chang (1991) showed that these misfits were due to statistically significant differences between the data flanking the Carlsberg Ridge and those flanking the Central Indian Ridge. The resulting pole of rotation between India and Australia since chron 5 is consistent with that found for present plate motion, but has huge uncertainties. The rotation between India and Australia since 20 Ma (chron 6) is marginally significantly larger than that since 11 Ma (chron 5) (Royer & Chang 1991).

The deformation of the equatorial Indian Ocean accommodates the motion of the Australian plate, as it subducts beneath the Sunda Trench, relative to the Indian plate, as it encounters resistance in its northward motion towards the Tibetan Plateau. The north–south to northwest–southeast convergence between the two plates east of the rotation pole, which is located just east of the Chagos–Laccadive Ridge, is taken up as distributed shortening. This area is thus an unusual and possibly unique laboratory to investigate the mechanical behaviour of the oceanic lithosphere that accommodates relative plate motion distributed over a wide zone.

Multichannel seismic profiles show that most of the horizontal shortening in the Central Indian Basin is accommodated by thrust faulting and particularly by deep thrust faults reaching the Moho and perhaps continuing into the upper mantle (Bull 1990; Chamot-Rooke *et al.* 1993). Strain estimated from the sum of the horizontal offsets of the thrust faults ranges from 1.2 to 4.3 per cent (Chamot-Rooke *et al.* 1993; Van Orman *et al.* 1995). In contrast, the large-scale deformations (long-wavelength undulations) accommodate less than 1 per cent of shortening (Gordon *et al.* 1990; Bull & Scrutton 1992).

Notwithstanding the considerable progress that has been made on the investigation of motion between the Australian and Indian plates, many important questions remain. Where does the boundary between India and Australia intersect the Central Indian or Carlsberg ridge? Is the boundary narrow or wide where it intersects the ridge? If wide, what are its northern and southern limits? What is the history of motion between the Indian and Australian plates? When did motion begin between the two plates? Has the pole of rotation remained in the same location? Has the rate of rotation varied with time? What is the total shortening indicated across the eastern deforming zone? How is the relative plate motion accommodated in the two deforming zones?

To answer these questions better, we undertook an aeromagnetic survey of the southern Carlsberg Ridge and northern Central Indian Ridge. Our survey filled a gap of more than 2000 km in the location of identifications of anomaly 5 and other anomalies that could be used in plate reconstructions. Here we present results for anomaly 5. In addition to the new crossings from the aeromagnetic survey, we use these data as an aid in identifying many other crossings of anomaly 5 from existing data. We determine a new set of fracture-zone crossings from satellite altimetry data. Our main goals include determination of a more accurate set of reconstructions for anomaly 5 that can be compared with present plate motions, and, in the case of motion between India and Australia, with independent indicators of the location and style of deformation. These accurate reconstructions can be used to calculate the integral of deformation on paths through the diffuse plate boundary connecting endpoints on each rigid plate. The new data are also used to address qualitative problems including the identification, location, and configuration of all fracture zones flanking the Carlsberg Ridge and Central Indian Ridge, and the age and tectonic origin of the seafloor flanking the ridges. The many data available give an opportunity to assess the dispersion and hence the accuracy in the location of magnetic-anomaly and fracture-zone crossings.

DATA

Magnetic-anomaly data

The aeromagnetic survey conducted in 1990 over the Central Indian Ridge (DeMets *et al.* 1994a) fills an important gap in magnetic data between 19°S and 5°N (*cf.* Royer & Chang 1991). For example, along the Indo–Australian side of the Carlsberg Ridge, the southernmost crossing used by Royer & Chang (1991) is at 5.4°N, 64.6°E, a few hundred kilometres northwest of the fracture zone labelled 'A' in Fig. 1. The northernmost crossing on the Indo–Australian side of the Central Indian Ridge used by Royer & Chang (1991) is at 13.6°S, 67.9°E, south of and near the Argo fracture zone. Along the African side of the Carlsberg Ridge, the southernmost crossing used by Royer & Chang (1991) is at 2.5°N, 63.3°E, a few tens of kilometres northwest of fracture zone A. The northernmost crossing on the African side of the Central Indian Ridge used by Royer & Chang (1991) is at 16.4°S, 65.6°E, between the Argo and Marie-Celeste fracture zones (Fig. 1). These data gaps of more than 2000 km are now well filled (Fig. 1). The aeromagnetic profiles were flown with the help of a tectonic lineation chart determined from the Geosat/GM (Geodetic Mission), and thus follow corridors between the many closely spaced fracture zones that offset the Central Indian and southern Carlsberg ridges (Figs 1 and 2). Originally we planned to combine these new data with the data compiled by Royer & Chang (1991), but the new aeromagnetic profiles helped us to identify for the first time many crossings of anomaly 5 from short or poorly oriented shipboard profiles (Fig. 2), as well as a few crossings from Project Magnet aeromagnetic profiles. Most of the shipboard magnetic profiles we used were obtained from the National Geophysical Data Center (NGDC) archives. The locations of additional magnetic crossings were digitized from published work including some analogue Project Magnet profiles (Fisher, Sclater & McKenzie 1971), Indian surveys along the Carlsberg Ridge (Chaubey

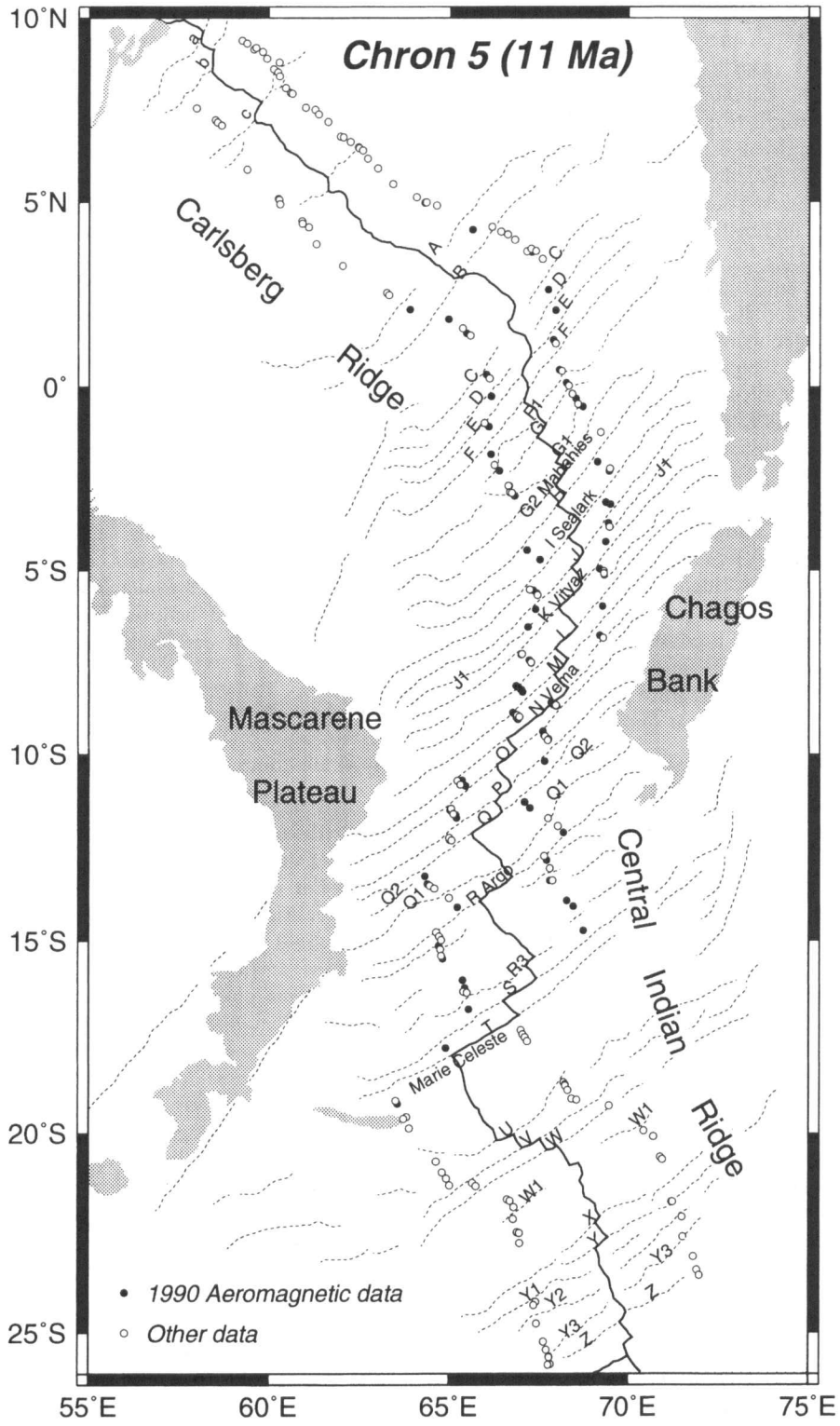

Figure 1. General tectonic chart showing the fracture-zone pattern, ridge axes and chron 5 (11 Ma) magnetic crossings compiled along the Carlsberg and Central Indian ridges. The ridge axes and fracture zones correspond to satellite-derived gravity troughs (grid from Smith & Sandwell 1995). Most of the critical data come from an aeromagnetic survey (solid circles) carried out in 1990 (DeMets *et al.* 1994a); open circles are crossings from other sources (Table 1). Stippled areas show the location of the Mascarene Plateau and Chagos–Laccadive Ridge.

et al. 1993) and along the Central Indian Ridge (Chaubey *et al.* 1990), and several French cruises (Tisseau 1978; Patriat 1987; Dyment 1991). Overall, we were able to compile 236 useful magnetic-anomaly crossings, including 86 from the 1990 aeromagnetic survey, 19 from Project Magnet flights, 72 from shipboard profiles in digital form from the NGDC, seven additional shipboard profiles in small-scale analogue form from other sources, and 56 from published work (Fig. 1,

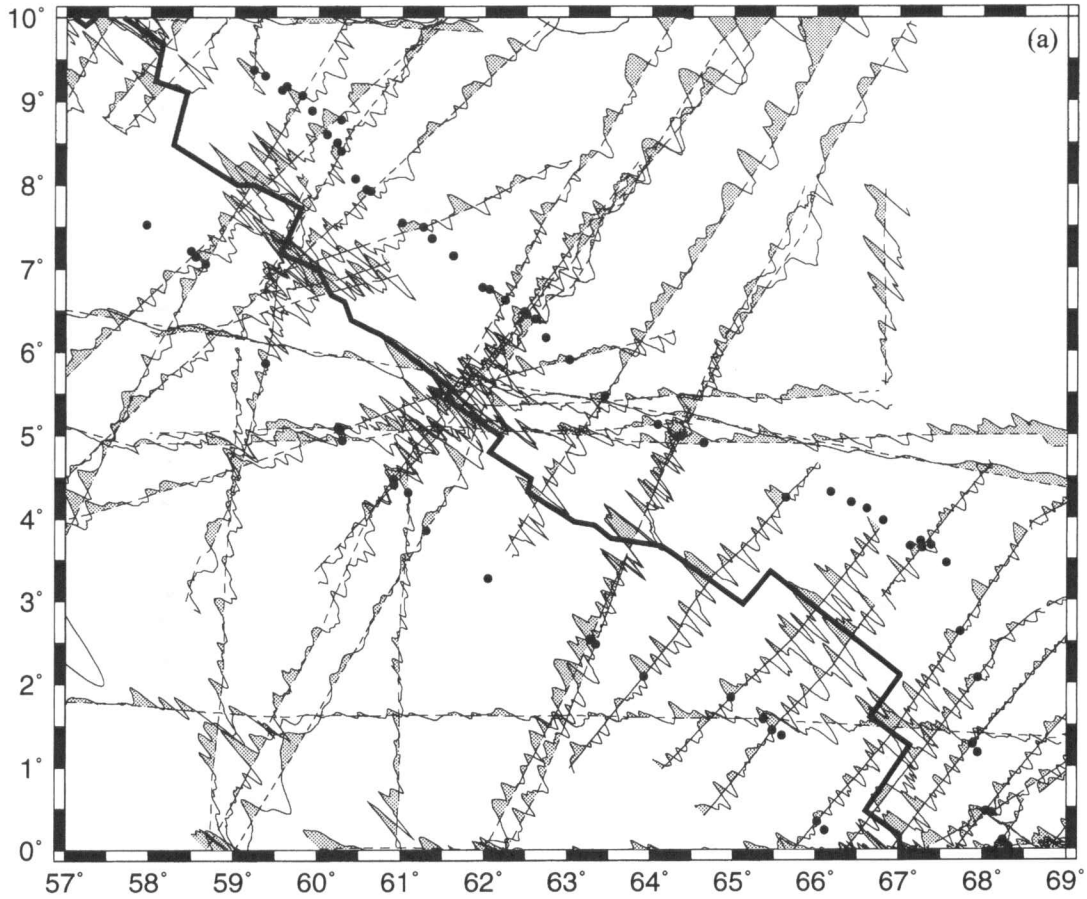

Figure 2. Aeromagnetic and shipboard magnetic profiles across the Central Indian and Carlsberg ridges. Dashed lines show tracks for shipboard cruises or Project Magnet flights. Solid lines show aeromagnetic tracks collected during a 1990 aeromagnetic survey (DeMets *et al.* 1994a). Small solid circles show the locations of anomaly 5 crossings used in this study. Circles not located along shiptracks or aeromagnetic tracks are taken from cruises unavailable to us in digital form. All magnetic profiles shown have been reduced to the pole, and for visual clarity are projected in a direction N45°W. Parts (a) to (e) progressively show magnetic profiles from the northwest to the southeast or south. A set of 18 closely spaced profiles in the region near the Vema fracture zone is omitted from part (c) but shown separately in part (f). The region shown in part (f) is outlined by heavy dashed lines in part (c).

Table 1). This is a substantial increase from the 79 crossings compiled and analysed by Royer & Chang (1991).

All the digital magnetic-anomaly profiles were reduced to the pole prior to their interpretation. The magnetic-anomaly crossings were extracted using an interactive computer program. DeMets *et al.* (1994) describe the processing of the magnetic profiles. We consistently picked the beginning (i.e. the old end) of anomaly 5. At a fast spreading centre the old end of anomaly 5 would correspond to the old end of chron 5n.2n of the geomagnetic reversal timescale of Cande & Kent (1995). Because of the slow spreading rate (~ 35 mm yr^{-1} full rate; Fig. 2) along the Carlsberg and Central Indian ridges, however, it is impossible to resolve a distinct anomaly corresponding to the slightly older normal polarity subchron 5r.1n. Thus it is unclear whether the age of the feature that we picked is that of the old end of chron 5r.1n (11.099 Ma) or, as seems more likely, the old end of chron 5n.2n (10.949 Ma).

The 56 crossings from prior work and the 79 crossings used by Royer & Chang (1991) both include 19 crossings from Russian work (Karasik *et al.* 1986). A close examination of the profiles presented in Glebovsky *et al.* (1995) shows that the anomaly crossings presented in figure 3 of Karasik *et al.* (1986) correspond to the centre of chron 5n, thus introducing a systematic bias of 0.7 Ma or about 9 km (at a half spreading rate of 13 to 14 km Myr^{-1}). Although their locations are listed in Table 1 and shown in some figures, we omitted them when determining the rotations and confidence limits presented herein.

Fracture-zone data

The well-developed fracture-zone pattern (Fig. 3a) helps to constrain the plate reconstructions. A set of discrete points from the palaeotransform faults near anomaly 5 is needed. Large offset fracture zones, such as the Mabahiss, Sealark, Vityaz, Vema, Argo, and Marie-Celeste, were mapped in the early 1970s (Engel & Fisher 1975; Fisher *et al.* 1971). Bathymetric soundings are generally too sparse, however, to map accurately the continuation of the fracture zones away from the ridge axis (Fisher, Jantsch & Comer 1982). This lack of information has now been overcome with the advent of satellite altimeters that provide a closely spaced and nearly uniform mapping of the geoid heights over most of the world ocean. Because the short wavelengths (<100 km) of the satellite-derived gravity reflect the uncompensated topography of the ocean floor, these data are useful for locating poorly

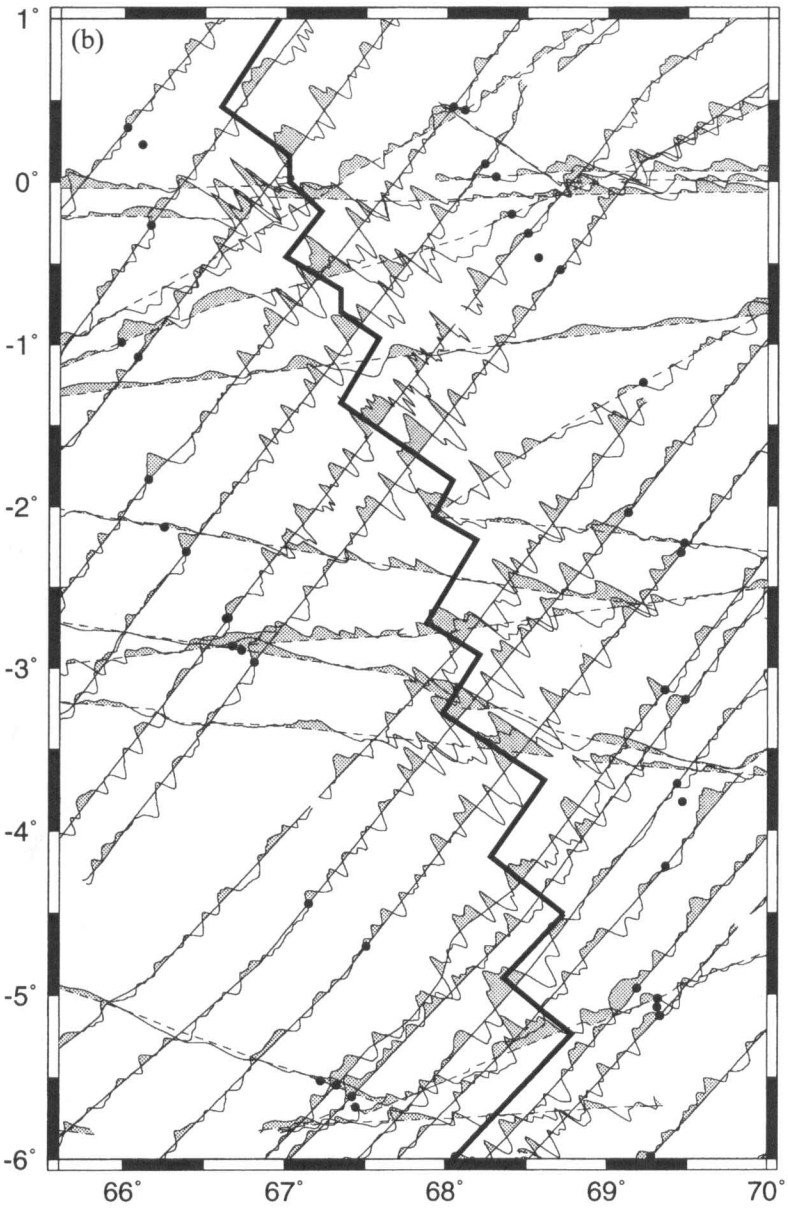

Figure 2. (*Continued.*)

charted or uncharted features of the seafloor such as fracture zones, ridges and plateaux (Sandwell 1984). Recently released Geosat/GM profiles and observations from the ERS-1 geodetic mission (168-day cycle) reveal new details of the seafloor tectonic fabric for the latitudes north of 30°S [i.e. north of the previously declassified Geosat/GM data (Fig. 3a; Smith & Sandwell 1995)].

To locate the fracture zones more precisely, we work from the satellite passes rather than from the gridded (hence interpolated or averaged) data. We use data from four altimeter satellites, Seasat, Geosat, Topex-Poseidon, and ERS-1, from profiles available to us during the summer of 1994. Because Topex-Poseidon and ERS-1 (35-day cycle) tracks have different orbit inclinations than do the Seasat and Geosat/ERM (Exact Repeat Mission) tracks, the combined tracks provide dense coverage. We use stacks of 44 repeat profiles of Geosat/ERM, 38 repeat profiles of Topex-Poseidon (Topex altimeter), and nine repeat profiles of ERS-1. Stacking improves the accuracy and resolution of altimetry measurements (e.g. Yale, Sandwell & Smith 1995). For each pass, geoid heights are converted into a vertical gravity anomaly (i.e. vertical component of the gravity along-track). The gravity profiles are then high- and low-pass filtered with Gaussian filters of the form $\exp(-t^2/2s^2)$, where t is time and s is the half-width of the filter in seconds. The effect of the filtering is to extract the short wavelengths (25–100 km; $s = 0.7$ s and $s = 2.8$ s, respectively) of the gravity field, which we assume represents the contribution of the uncompensated topography.

The Central Indian and Carlsberg ridges have been slowly spreading since Middle Eocene times (Patriat 1987; Fisher *et al.* 1971), thus each fracture zone is expressed as a deep valley as in the Atlantic Ocean. Because the gravity troughs appear to coincide with fracture-zone troughs, the traces of the fracture zones can be mapped using the satellite-derived

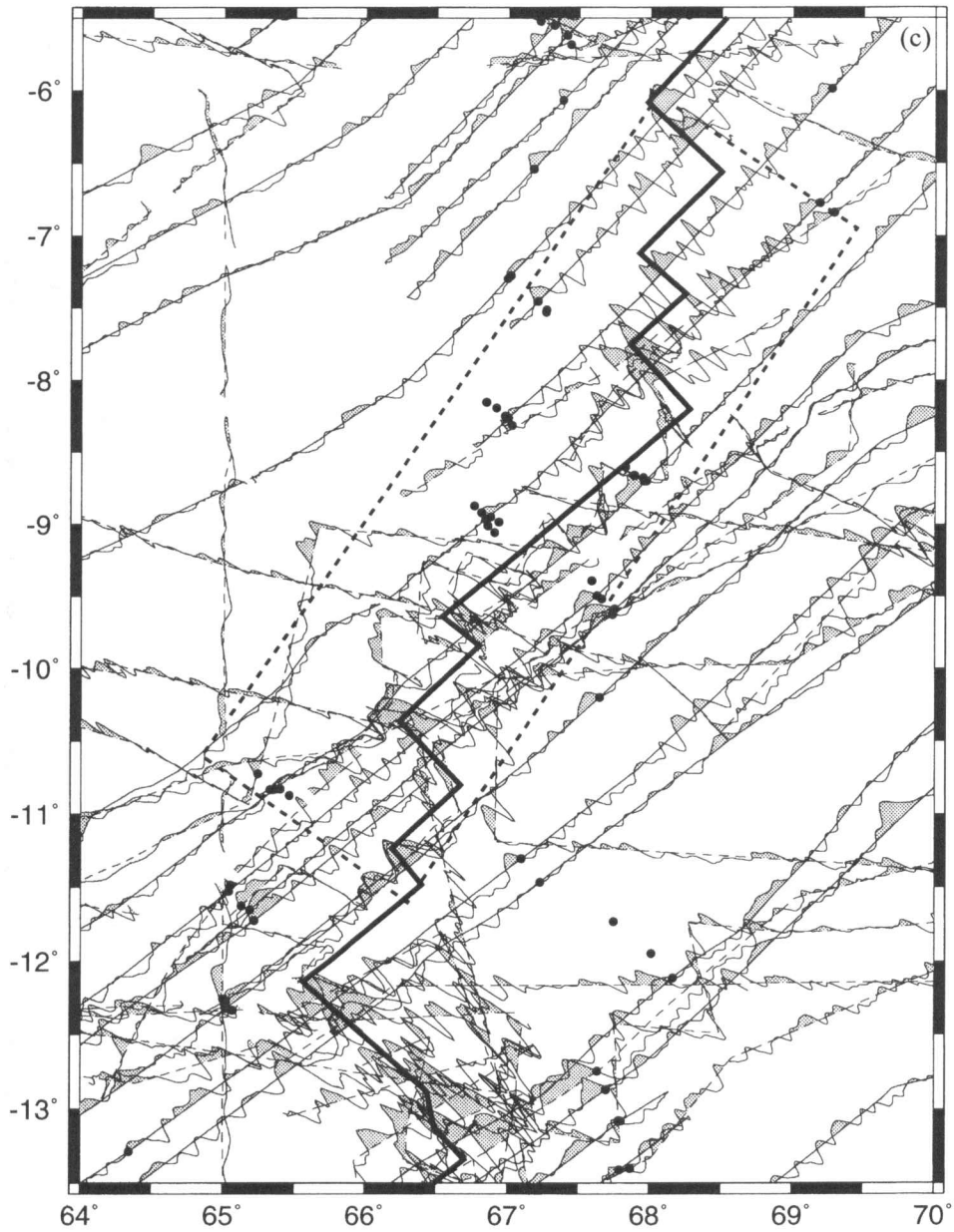

Figure 2. (*Continued.*)

gravity anomalies (Müller *et al.* 1991; Müller & Roest 1992). For this study we systematically searched for gravity troughs along the ascending and descending passes of each altimeter satellite (Fig. 3b). The characteristic signature of the fracture zones and the close spacing of the tracks enabled us to select 177 fracture-zone crossings from 22 conjugate palaeotransform faults near anomaly 5 (Table 2), which is many more than the 23 fracture-zone crossings of Royer & Chang (1991).

Is the present geometry of fracture-zone segments representative of the geometry of the plate boundary for a moment in the distant past? Any change in the direction of plate motion since the time of interest will modify the shape of a fracture zone. This effect will be even more important if the transform offset is large and will not be recorded symmetrically on conjugate fracture zones, hence we avoided using fracture zones with offsets larger than 100 km (6 Myr offset at 17 mm yr^{-1} half-rate). As is shown below, the Africa–India and Africa–Australia poles of rotation have moved little during the past 11 Myr, thus the fracture-zone crossings are unlikely to have been greatly disturbed by the tectonic noise caused by a change in the direction of plate motion.

Summary of data available for plate reconstructions

A total of 413 magnetic-anomaly and fracture-zone crossings are used to improve the Africa–India–Australia plate reconstructions, with 210 data points from the African plate and 203 from the Indo–Australian side of the Central Indian and Carlsberg ridges. These data are divided into 63 segments corresponding to conjugate magnetic lineations or palaeotransform faults. A few corridors, where data are lacking on one side of the ridge system [e.g. segment number 2 (as identified in Table 1)] or where there is only one crossing on each side of the ridge (e.g. segment numbers 7, 10 and 20),

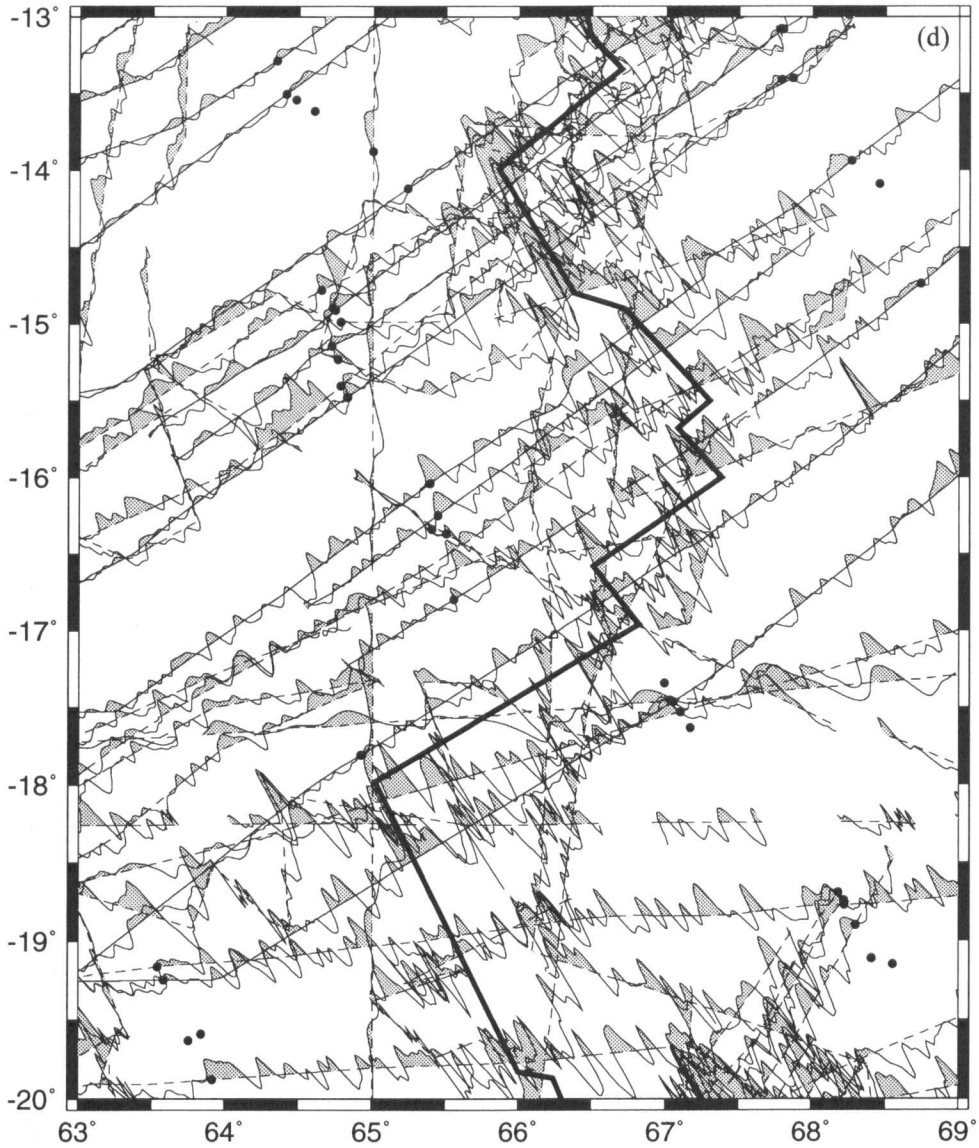

Figure 2. (*Continued.*)

have too few data to be used in the inversion for reconstruction parameters. In addition, a few questionable magnetic-anomaly identifications (listed with stars in Table 1) are discarded. Overall, only 377 crossings (396 crossings with the Russian data) defining 54 different segments are potentially usable for estimating plate-rotation parameters.

UNCERTAINTIES

Magnetic-anomaly crossings

For the magnetic-anomaly data, the sources of error in the location of the anomaly crossings are uncertainties in navigation, the limitations of the fidelity of the seafloor as a magnetic recorder, the loss of resolution that occurs from measuring the magnetic field several kilometres above the seafloor, and ambiguities in location caused by the skewness of an anomaly. We suspect that the dominant errors are navigation and fidelity of the seafloor magnetic recorder. This belief led us to divide the data into four categories, A, B, C and D, based mainly on the quality of the navigation. The A category initially included data since 1985, which in many cases used GPS navigation. The B category initially included all cruises from 1980 to 1985, which typically used partial GPS and Transit satellites. The C category initially included all cruises from the 1970s, which relied mainly on Transit satellites. The D label initially included all pre-1970 cruises, which lacked satellite navigation. A crossing was usually demoted by one or more categories if unavailable to us in digital form and in some cases demoted if it was of low quality (e.g. anomaly poorly shaped, proximity to a fracture zone). Our prejudice is that the 'A' data should have smaller uncertainties than the 'B' data, which should have smaller uncertainties than the 'C' data, etc. It is more difficult to determine what these uncertainties are.

Fracture-zone crossings

Several factors contribute to uncertainties in fracture-zone locations. First, even with excellent bathymetric or gravity data, one cannot determine where in the fracture-zone valley,

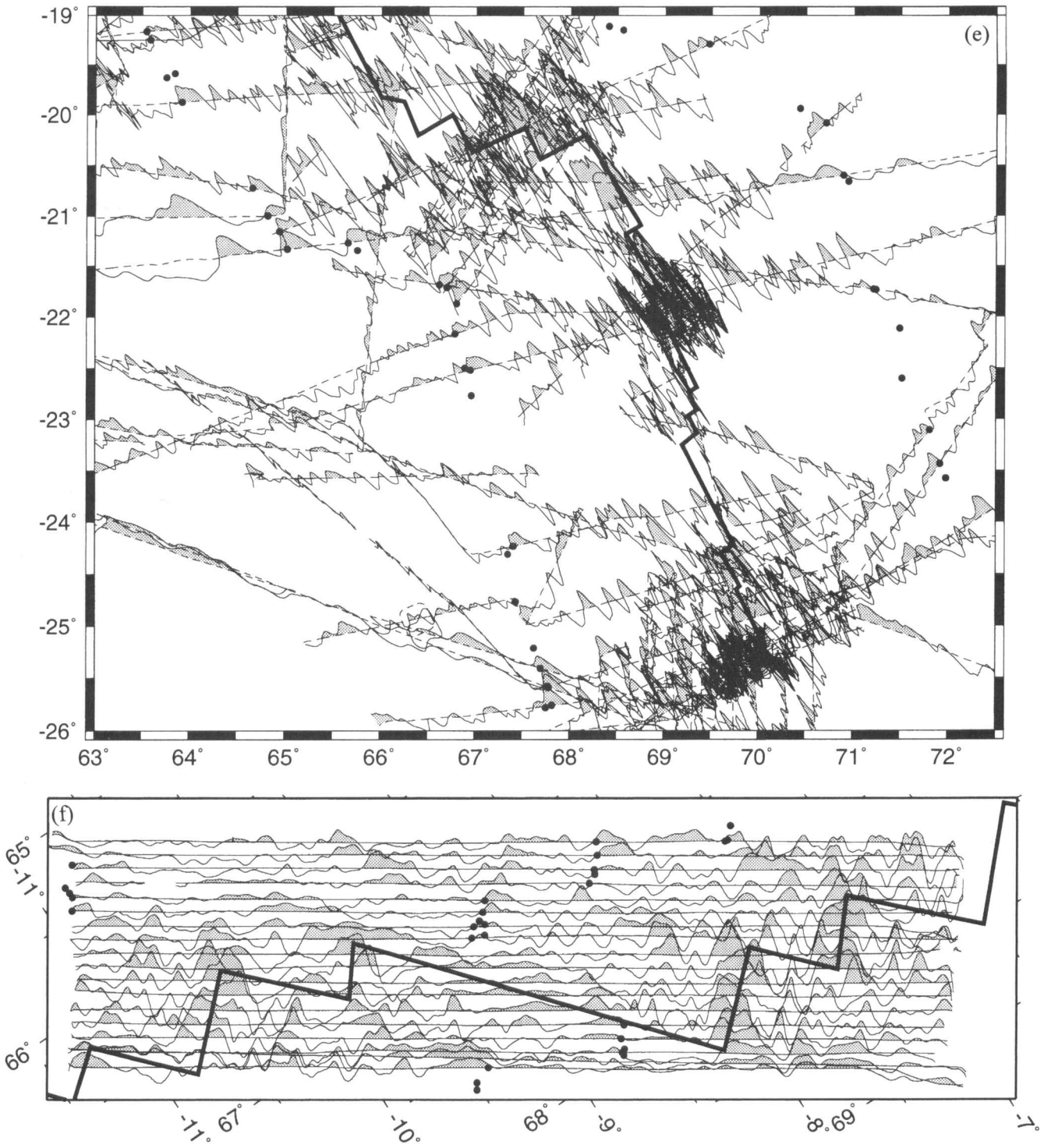

Figure 2. (*Continued.*)

which can be up to several tens of kilometres wide, is the trace of the transform fault that was active at a particular moment in the past. Second, shipboard and satellite-derived data have navigation errors, which are difficult to quantify. Third, shipboard bathymetric data and especially satellite-derived gravity data have less resolution than would be available from an accurate image of the subsediment topography. In so far as both navigation errors and resolution errors are uncorrelated among different locations, their magnitude can be estimated from the dispersion of the location of fracture-zone crossings about great circle segments. The effect of these errors on the estimated rotations diminishes with increasing numbers of crossings. One must also be concerned, however, especially in using satellite-derived gravity, about errors that do not diminish with increasing numbers of crossings, in particular for consistent offsets of the gravity troughs relative to the bathymetric troughs.

A comparison of the filtered geoid height (25–100 km

Table 1. Chron 5 magnetic-anomaly crossings [chron 5n.2n from Cande & Kent (1995) magnetic reversal timescale].

Latitude [°N]	Longitude [°E]	Segment number	Plate	Quality	Year	Ship (cruise) / Flight	Source
9.373	59.236	1	in	B	1987	D/V Joides Resolution (Leg 117)	NGDC
9.300	59.366	1	in	D†a*	1980		Karasik *et al.* (1986)
9.132	59.564	1	in	D†a*	1980		Karasik *et al.* (1986)
9.178	59.622	1	in	Ca*	1965	R/V Atlantis (Leg 2152)	NGDC
9.069	59.813	1	in	D	1962	HMS Owen (Leg 3)	NGDC
8.886	59.923	1	in	D†a*	1980		Karasik *et al.* (1986)
8.781	60.274	1	in	D*	1989	R/V Sagar Kanya (Leg 50-03)	Chaubey *et al.* (1993)
7.527	57.969	1	af	Ca*	1977	N.O. Suroit (Leg 3-18)	Tisseau (1978)
7.214	58.491	1	af	Ca*	1977	N.O. Suroit (Leg 3-17)	Tisseau (1978)
7.146	58.550	1	af	D	1989	R/V Sagar Kanya (Leg 50-03)	Chaubey *et al.* (1993)
7.059	58.662	1	af	D	1962	HMS Owen (Leg 3)	NGDC
8.601	60.107	2	in	D†a*	1980		Karasik *et al.* (1986)
8.505	60.230	2	in	D†a*	1980		Karasik *et al.* (1986)
8.404	60.276	2	in	B*	1978	USNS Wilkes (Leg 821)	NGDC
8.074	60.448	3	in	D†a*	1980		Karasik *et al.* (1986)
7.945	60.575	3	in	D†a*	1980		Karasik *et al.* (1986)
7.925	60.628	3	in	D	1989	R/V Sagar Kanya (Leg 50-01)	Chaubey *et al.* (1993)
7.549	61.003	3	in	D†a*	1980		Karasik *et al.* (1986)
7.500	61.265	3	in	D	1963	R/V Vema (Leg 1910)	NGDC
7.360	61.363	3	in	D†a*	1980		Karasik *et al.* (1986)
7.156	61.623	3	in	D†a*	1980		Karasik *et al.* (1986)
5.864	59.378	3	af	B	1977	R/V Vema (Leg 3407)	NGDC
5.086	60.244	3	af	D	1965	R/V Atlantis (Leg 1503)	NGDC
5.057	60.271	3	af	C	1977	R/V Melville (Exp. Indomed 04)	NGDC
4.938	60.295	3	af	D	1963	R/V Atlantis (Leg 802)	NGDC
6.770	61.971	4	in	D†a*	1980		Karasik *et al.* (1986)
6.751	62.055	4	in	D†a*	1980		Karasik *et al.* (1986)
6.619	62.252	4	in	B	1978	USNS Wilkes (Leg 827)	NGDC
6.482	62.482	4	in	B	1977	R/V Vema (Leg 3408)	NGDC
6.447	62.508	4	in	D	1962	HMS Owen (Leg 6)	NGDC
6.391	62.606	4	in	B	1988	Project Magnet (Flt 5072.2)	NGDC
6.164	62.735	4	in	D†a*	1980		Karasik *et al.* (1986)
5.902	63.017	4	in	B	1977	R/V Melville (Exp. Indomed 04)	NGDC
5.476	63.448	4	in	D	1962	HMS Owen (Leg 6)	NGDC
4.479	60.907	4	af	B	1977	R/V Vema (Leg 3408)	NGDC
4.412	60.916	4	af	D	1962	HMS Owen (Leg 6)	NGDC
4.317	61.086	4	af	D	1963	R/V Argo (Leg 7a)	NGDC
3.273	62.044	4	af	D	1962	HMS Owen (Leg 6)	NGDC
3.856	61.304	5	af	B*	1988	Project Magnet (Flt 5072.2)	NGDC
5.124	64.084	6	in	D	1965	R/V Atlantis (Leg 1503)	NGDC
4.975	64.314	6	in	C	1974	R/V Robert Conrad (Leg 1707)	NGDC
4.985	64.363	6	in	D	1962	HMS Owen (Leg 1)	NGDC
4.901	64.641	6	in	D	1963	R/V Atlantis (Leg 802)	NGDC
2.535	63.269	6	af	D	1962	HMS Owen (Leg 1)	NGDC
2.480	63.339	6	af	C	1974	R/V Robert Conrad (Leg 1707)	NGDC
2.087	63.919	7	af	A*	1990	DG (Flt 3.15N)	This paper
4.253	65.636	7	in	A*	1990	DG (Flt 3.15N)	This paper
4.322	66.178	8	in	D†a*	1980		Karasik *et al.* (1986)
4.196	66.422	8	in	D†a*	1980		Karasik *et al.* (1986)
4.122	66.614	8	in	D†a*	1980		Karasik *et al.* (1986)
3.977	66.804	8	in	D†a*	1980		Karasik *et al.* (1986)

Table 1. (*Continued.*)

3.662	67.132	8	in	D†a*	1980		Karasik *et al.* (1986)
3.726	67.255	8	in	A	1988	M/S Marion Dufresne (Leg 57-63)	Dyment (1991)
3.636	67.277	8	in	A	1990	DG (Flt 2.60N)	This paper
3.672	67.382	8	in	A	1988	M/S Marion Dufresne (Leg 57-61)	Dyment (1991)
3.458	67.567	8	in	D†a*	1980		Karasik *et al.* (1986)
1.833	64.977	8	af	A	1990	DG (Flt 2.90N)	This paper
1.579	65.363	8	af	D	1971	R/V Chain (Leg 100-5)	NGDC
1.445	65.477	8	af	A	1990	DG (Flt 2.60N)	This paper
1.380	65.589	8	af	A	1988	M/S Marion Dufresne (Leg 57-63)	Dyment (1991)
2.625	67.733	9	in	A	1990	DG (Flt 1.45N)	This paper
0.332	66.017	9	af	B	1990	DG (Flt 1.45N)	This paper
0.230	66.109	9	af	Ba*	1979	USNS Wilkes (Leg 907)	NGDC
2.069	67.942	10	in	A*	1990	DG (Flt 1.05N)	This paper
-0.266	66.164	10	af	A*	1990	DG (Flt 1.05N)	This paper
1.275	67.878	11	in	A	1990	DG (Flt 0.15N)	This paper
1.171	67.940	11	in	Ba*	1979	USNS Wilkes (Leg 907)	NGDC
-0.986	65.981	11	af	B	1979	USNS Wilkes (Leg 915)	NGDC
-1.078	66.085	11	af	A	1990	DG (Flt 0.15N)	This paper
0.438	68.114	12	in	C	1971	R/V Melville (Exp. Antipode 10)	NGDC
0.458	68.040	12	in	A	1990	DG (Flt 0.50S)	This paper
-1.833	66.152	12	af	A	1990	DG (Flt 0.50S)	This paper
0.112	68.240	13	in	A	1990	DG (Flt 0.90S)	This paper
0.032	68.307	13	in	D	1963	R/V Argo (Leg 7c)	NGDC
-2.127	66.248	13	af	D	1969	R/V Umitaka (Leg 68)	NGDC
-2.281	66.382	13	af	A	1990	DG (Flt 0.90S)	This paper
-0.196	68.406	14	in	B	1979	USNS Wilkes (Leg 915)	NGDC
-0.314	68.503	14	in	A	1990	DG (Flt 1.50S)	This paper
-2.695	66.632	14	af	A	1988	M/S Marion Dufresne (Leg 57-67)	Dyment (1991)
-2.691	66.648	14	af	C	1990	DG (Flt 1.50S)	This paper
-0.466	68.568	15	in	A	1988	M/S Marion Dufresne (Leg 57-67)	Dyment (1991)
-0.538	68.704	15	in	C	1990	DG (Flt 1.70S)	This paper
-2.865	66.670	15	af	D	1969	R/V Robert Conrad (Leg 1215)	NGDC
-2.892	66.731	15	af	B	1986	Project Magnet (Flt 5059A)	NGDC
-2.964	66.808	15	af	A	1990	DG (Flt 1.70S)	This paper
-1.234	69.220	16	in	D*	1964	R/V Argo (Exp. Dodo 8)	NGDC
-2.040	69.128	17	in	B	1990	DG (Flt 3.30S)	This paper
-2.228	69.477	17	in	C	1964	R/V Argo (Exp. Dodo 8)	NGDC
-2.288	69.458	17	in	D	1990	DG (Flt 3.50S)	This paper
-4.444	67.146	17	af	A	1990	DG (Flt 3.30S)	This paper
-4.707	67.504	17	af	D	1990	DG (Flt 3.50S)	This paper
-3.138	69.359	18	in	A	1990	DG (Flt 4.30S)	This paper
-3.197	69.487	18	in	A	1990	DG (Flt 4.42S)	This paper
-5.521	67.219	18	af	C	1988	Project Magnet (Flt 5072)	NGDC
-5.549	67.319	18	af	A	1990	DG (Flt 4.30S)	This paper
-5.619	67.415	18	af	A	1990	DG (Flt 4.42S)	This paper
-5.681	67.439	18	af	D	1964	R/V Argo (Exp. Dodo 8)	NGDC
-3.711	69.435	19	in	A	1990	DG (Flt 4.95S)	This paper
-3.823	69.466	19	in	D	1962	HMS Owen (Leg 2)	NGDC
-6.067	67.384	19	af	A	1990	DG (Flt 4.95S)	This paper
-4.217	69.361	20	in/au	A*	1990	DG (Flt 5.08 D	This paper
-6.541	67.176	20	af	A*	1990	DG (Flt 5.08S)	This paper
-4.962	69.185	21	in/au	A	1990	DG (Flt 6.19S)	This paper
-5.023	69.312	21	in/au	C	1964	R/V Argo (Exp. Dodo 8)	NGDC
-5.077	69.312	21	in/au	B	1980	M/S Marion Dufresne (Leg 23-03)	Patriat (1987)
-5.129	69.330	21	in/au	A	1990	DG (Flt 6.30S)	This paper
-7.277	67.018	21	af	A	1988	M/S Marion Dufresne (Leg 57-43)	Dyment (1991)

Table 1. (*Continued.*)

-7.295	66.994	21	af	A	1990	DG (Flt 6.19S)	This paper
-7.453	67.207	21	af	B	1990	DG (Flt 6.30S)	This paper
-7.511	67.267	21	af	B	1980	M/S Marion Dufresne (Leg 23)	Patriat (1987)
-7.529	67.263	21	af	A	1990	DG (Flt 11.1D)	This paper
-5.985	69.275	22	in/au	A	1990	DG (Flt 7.25S)	This paper
-8.150	66.847	22	af	B	1990	DG (Flt 11.1D)	This paper
-8.189	66.916	22	af	A	1990	DG (Flt 11.2D)	This paper
-8.246	66.975	22	af	A	1990	DG (Flt 11.3D)	This paper
-8.259	67.001	22	af	A	1990	DG (Flt 7.25S)	This paper
-8.314	67.026	22	af	A	1990	DG (Flt 11.4D)	This paper
-6.773	69.191	23	in/au	A	1990	DG (Flt 7.95S)	This paper
-6.840	69.290	23	in/au	D	1964	R/V Argo (Exp. Dodo 8)	NGDC
-8.871	66.762	23	af	A	1990	DG (Flt 11.5D)	This paper
-8.917	66.812	23	af	A	1990	DG (Flt 11.6D)	This paper
-8.948	66.878	23	af	B	1988	M/S Marion Dufresne (Leg 57-37)	Dyment (1991)
-8.983	66.932	23	af	Da*	1962	HMS Owen (Leg 2)	NGDC
-8.963	66.844	23	af	B	1990	DG (Flt 7.95S)	This paper
-9.009	66.855	23	af	A	1990	DG (Flt 12.1D)	This paper
-9.057	66.903	23	af	A	1990	DG (Flt 12.2D)	This paper
-8.602	67.827	24	in/au	B	1990	DG (Flt 13.2D)	This paper
-8.659	67.887	24	in/au	A	1990	DG (Flt 13.3D)	This paper
-8.677	67.949	24	in/au	C	1971	R/V Melville (Exp. Antipode 08)	NGDC
-8.699	67.975	24	in/au	A	1990	DG (Flt 9.75S)	This paper
-8.698	67.957	24	in/au	A	1990	DG (Flt 13.6D)	This paper
-10.711	65.364	24	af	C*	1990	DG (Flt 11.4D)	This paper
-10.723	65.240	24	af	D	1968	R/V Argo (Exp. Circe 06)	NGDC
-10.826	65.396	24	af	B	1990	DG (Flt 11.5D)	This paper
-10.826	65.364	24	af	A	1990	DG (Flt 9.75S)	This paper
-10.830	65.326	24	af	B	1988	Project Magnet (Flt 5073)	NGDC
-10.871	65.460	24	af	B	1990	DG (Flt 11.6D)	This paper
-9.391	67.589	25	au	A	1990	DG (Flt 13.5D)	This paper
-9.493	67.626	25	au	A	1990	DG (Flt 10.5S)	This paper
-9.518	67.661	25	au	Ba*	1977	M/S Marion Dufresne (Leg15-12)	Patriat (1987)
-9.588	67.752	25	au	A	1990	DG (Flt 10.6S)	This paper
-9.601	67.739	25	au	B	1988	Project Magnet (Flt 5073)	NGDC
-9.627	67.737	25	au	C	1971	R/V Melville (Exp. Antipode 08)	NGDC
-11.482	65.055	25	af	D	1964	R/V Argo (Exp. Dodo 8)	NGDC
-11.525	65.040	25	af	A	1990	DG (Flt 10.5S)	This paper
-11.622	65.127	25	af	C	1971	R/V Melville (Exp. Antipode 08)	NGDC
-11.650	65.186	25	af	A	1990	DG (Flt 10.6S)	This paper
-11.727	65.216	25	af	A	1990	DG (Flt 10.6Sp)	This paper
-10.198	67.646	26	au	A	1990	DG (Flt 11.4Sp)	This paper
-12.258	65.001	26	af	C	1986	Project Magnet (Flt 5067.2)	NGDC
-12.269	65.021	26	af	A	1990	DG (Flt 11.4Sp)	This paper
-12.320	65.020	26	af	A	1990	DG (Flt 11.4S)	This paper
-12.332	65.067	26	af	C	1970	R/V Chain (Leg 9905)	NGDC
-11.302	67.095	27	au	A	1990	DG (Flt 12.3S)	This paper
-11.462	67.227	27	au	B	1990	DG (Flt 12.4S)	This paper
-13.288	64.345	27	af	A	1990	DG (Flt 12.3S)	This paper
-13.506	64.409	27	af	A	1990	DG (Flt 12.4S)	This paper
-13.542	64.478	27	af	Da*	1962	HMS Owen (Leg2)	NGDC
-13.615	64.604	27	af	A	1988	M/S Marion Dufresne (Leg 57-27)	Dyment (1991)
-11.732	67.747	28	au	A*	1988	M/S Marion Dufresne (Leg 57-27)	Dyment (1991)
-11.949	68.013	28	au	A	1988	M/S Marion Dufresne (Leg 57-25)	Dyment (1991)
-12.115	68.165	28	au	A	1990	DG (Flt 13.25S)	This paper
-13.877	65.001	28	af	B	1986	Project Magnet (Flt 5067.2)	NGDC

Table 1. (*Continued.*)

-14.120	65.237	28	af	A	1990	DG (Flt 13.25S)	This paper
-12.746	67.632	29	au	C	1972	D/V Glomar Challenger (Leg 24)	NGDC
-12.869	67.698	29	au	A	1990	DG (Flt 14.10S)	This paper
-13.078	67.784	29	au	C	1971	R/V Melville (Exp. Antipode 08-4)	NGDC
-13.082	67.799	29	au	B	1990	DG (Flt 14.25S)	This paper
-14.779	64.653	29	af	C	1972	D/V Glomar Challenger (Leg 24)	NGDC
-14.892	64.730	29	af	C	1971	R/V Melville (Exp. Antipode 08-6)	NGDC
-14.908	64.750	29	af	B	1990	DG (Flt 14.10S)	This paper
-14.988	64.785	29	af	D	1968	R/V Argo (Exp. Circe 06)	NGDC
-13.411	67.791	30	au	B	1990	DG (Flt 14.50S)	This paper
-13.403	67.866	30	au	C	1971	R/V Melville (Exp. Antipode 08)	NGDC
-15.145	64.724	30	af	B	1990	DG (Flt 14.25S)	This paper
-15.233	64.766	30	af	C	1971	R/V Melville (Exp. Antipode 08-7)	NGDC
-15.404	64.785	30	af	C	1971	R/V Melville (Exp. Antipode 08-6)	NGDC
-15.479	64.828	30	af	B	1990	DG (Flt 14.50S)	This paper
-13.937	68.268	31	au	A	1990	DG (Flt 15.03S)	This paper
-14.087	68.456	31	au	A	1990	DG (Flt 15.20S)	This paper
-16.041	65.390	31	af	B	1990	DG (Flt 15.03S)	This paper
-16.249	65.444	31	af	A	1990	DG (Flt 15.20S)	This paper
-16.341	65.404	31	af	D	1990	Project Magnet (Flt 515C)	Fisher *et al.* (1971)
-16.370	65.503	31	af	D	1964	R/V Argo (Exp. Dodo 8)	NGDC
-14.735	68.739	32	au	C*	1990	DG (Flt 15.80S)	This paper
-16.797	65.555	32	af	A*	1990	DG (Flt 15.80S)	This paper
-17.809	64.922	33	af	B*	1990	DG (Flt 16.75S)	This paper
-17.454	67.034	34	au	B	1986	Project Magnet (Flt 5057)	NGDC
-17.460	67.051	34	au	A	1990	DG (Flt 18.45S)	This paper
-17.529	67.100	34	au	C	1967	R/V Vema (Leg 2410)	NGDC
-17.631	67.167	34	au	D	1970	R/V Melville (Exp. Antipode 06)	NGDC
-19.163	63.540	34	af	C	1970	R/V Melville (Exp. Antipode 05)	NGDC
-19.247	63.582	34	af	A	1990	DG (Flt 18.45S)	This paper
-19.590	63.840	34	af	Ca*	1970	M/S Galliéni (Leg 03-39)	Patriat (1987)
-19.631	63.751	34	af	D	196?	Project Magnet (Flt 516B)	Fisher *et al.* (1971)
-19.879	63.916	34	af	C	1968	R/V Argo (Exp. Circe 07)	NGDC
-18.691	68.180	35	au	B	198?	R/V Sagar Kanya (Leg 20-03)	Chaubey *et al.* (1990)
-18.740	68.220	35	au	B	198?	R/V Sagar Kanya (Leg 20-02)	Chaubey *et al.* (1990)
-18.770	68.224	35	au	C	1970	R/V Melville (Exp. Antipode 05)	NGDC
-18.898	68.301	35	au	B	198?	R/V Sagar Kanya (Leg 20-01)	Chaubey *et al.* (1990)
-19.109	68.405	35	au	D	196?	Project Magnet (Flt 516B)	Fisher *et al.* (1971)
-19.146	68.553	35	au	A	1988	M/S Marion Dufresne (Leg 57-09)	Dyment (1991)
-20.723	64.661	35	af	C	1962	R/V Vema (Leg 1811)	NGDC
-21.001	64.818	35	af	B	1986	Project Magnet (Flt 5067)	NGDC
-21.153	64.940	35	af	C	1972	R/V Vema (Leg 2903)	NGDC
-21.329	65.023	35	af	C	1988	Project Magnet (Flt 5022.1)	NGDC
-19.291	69.469	36	au	C	1972	R/V Vema (Leg 2903)	NGDC
-21.265	65.657	36	af	B	1988	Project Magnet (Flt 5022.1)	NGDC
-21.342	65.758	36	af	A	1988	M/S Marion Dufresne (Leg 57-02)	Dyment (1991)
-21.685	66.619	37	af	C*	1968	R/V Argo (Exp. Circe 07)	NGDC
-21.711	66.697	37	af	C*	198?	R/V Sagar Kanya (Leg 16-02)	Chaubey *et al.* (1990)
-21.870	66.802	37	af	C*	198?	R/V Sagar Kanya (Leg 16-03)	Chaubey *et al.* (1990)
-19.940	70.434	38	au	A	1988	M/S Marion Dufresne (Leg 57-07)	Dyment (1991)
-20.081	70.709	38	au	D	1964	R/V Argo (Exp. Dodo 8)	NGDC
-22.166	66.784	38	af	C	1976	R/V Atlantis (Leg 2093)	NGDC
-22.500	66.890	38	af	D	1976	R/V Atlantis (Leg 2035)	NGDC
-22.520	66.951	38	af	C	1964	R/V Vema (Leg 2009)	NGDC
-20.598	70.897	39	au	B	1988	Project Magnet (Flt 5022.1)	NGDC
-20.660	70.950	39	au	Ca*	1980	M/S Marion Dufresne (Leg 23-14)	Patriat (1987)

Table 1. (*Continued.*)

-22.769	66.957	39	af	Da*	1968	R/V Argo (Exp. Circe 05)	NGDC
-21.730	71.216	40	au	D	1962	R/V Vema (Leg 1811)	NGDC
-21.735	71.240	40	au	A	1984	N.O. Jean Charcot (Leg 03-11)	NGDC
-22.112	71.495	40	au	D	196?	Project Magnet (Flt 818)	Fisher *et al.* (1971)
-24.233	67.407	40	af	C	1994	R/V Atlantis (Leg 2093)	NGDC
-24.310	67.350	40	af	C	1975	M/S Marion Dufresne (Leg 6)	Patriat (1987)
-22.605	71.518	41	au	D	196?	Project Magnet (Flt 541)	Fisher *et al.* (1971)
-23.105	71.811	41	au	B	1987	RRS Charles Darwin (Leg 2387-6)	NGDC
-23.437	71.918	41	au	A	1987	RRS Charles Darwin (Leg 2387-5)	NGDC
-23.578	71.980	41	au	Da*	1968	R/V Argo (Exp. Circe 5)	Fisher *et al.* (1971)
-24.767	67.431	41	af	Da*	1968	M/S Galliéni (Leg 01-03)	Patriat (1987)
-25.217	67.625	41	af	Da*	1968	M/S Galliéni (Leg 01-01)	Patriat (1987)
-25.411	67.698	41	af	B	1988	Project Magnet (Flt 5022.2)	NGDC
-25.582	67.774	41	af	D	1960	R/V Argo (Exp. Monsoon 4)	NGDC
-25.592	67.781	41	af	B	1988	Project Magnet (Flt 5090)	NGDC
-25.763	67.818	41	af	B	1987	RRS Charles Darwin (Leg 2387-7)	NGDC
-25.782	67.753	41	af	Ba*	1980	M/S Marion Dufresne (Leg 23)	Patriat (1987)

Picks are sorted by segment number and by plates (af = Africa, in = India, au = Australia). Quality of data expressed reliability of navigation and/or of magnetic anomaly identification (from A—best to D—worst, see text). Symbols denote (*) data that were not used in our inversions, (a) picks digitized from analogue data record, (†) picks corresponding to the middle of chron 5n.2 from Karasik *et al.* (1986).

wavelengths) measured by Geosat with the basement topography along the Kane fracture zone indicates that the geoid troughs lie within 10 km of the basement troughs on 33 of 37 Geosat profiles (Müller *et al.* 1991). These 33 profiles have a mean mismatch between geoid and basement of about 5 km. The other four profiles either cross the transverse ridge east of the active Kane transform fault or overlie old crust of the M-anomaly sequence, where the control on basement is poor. Given that the Carlsberg and Central Indian ridges are Atlantic-type spreading ridges, we build on the result from Müller *et al.* (1991) and assign 1σ uncertainties of 5 km, corresponding to 95 per cent confidence limits of 9.8 km, to our fracture-zone crossings. The real errors may be much larger. Only further investigation of fracture-zone crossings from satellite geoid data, beyond the scope of the present paper, will firmly establish the real size of the errors.

METHODS

Plate reconstructions and dispersion of the data

To determine the best-fitting rotations matching the magnetic-anomaly and fracture-zone data from a conjugate pair of plates, we follow Royer & Chang (1991) in using the algorithms developed by Chang (1987, 1988). The data are divided into conjugate segments, each representing a great-circle-like portion of a magnetic lineation or a fracture zone. A segment is defined by at least three points with at least two from one plate and at least one from the other. The misfit is the sum of the squared normalized distances between each datum and the mean great circle approximating the segment. Each distance is normalized by dividing by the uncertainty assigned to the corresponding datum. Each assigned uncertainty is an estimate of the 1-D standard deviation in the location of a crossing. The best-fitting rotation minimizes Hellinger's (1981) criterion of fit. The uncertainties in the best-fitting rotation, typically parametrized as the angle of rotation and the latitude and longitude of the Euler pole, are described by a covariance matrix propagated from the uncertainties assigned to the data. The quality of the best-fitting rotation and its uncertainties thus depends on the errors assigned to the data.

Chang's algorithms require only that the ratios of the uncertainties assigned to the data be correct, and permit them to be systematically too high or too low by a uniform multiplicative constant. The covariance matrix determined from the assigned uncertainties can be rescaled by dividing by $\hat{\kappa}$, which equals the number of degrees of freedom divided by the sum-squared normalized misfit and is a measure of the average ratio of the square of an assigned uncertainty to the square of the misfit to the corresponding datum. The number of degrees of freedom in turn equals $N - 2s - 3$, where N is the total number of data inverted and s is the total number of segments. A value of $\hat{\kappa}$ near 1 is consistent with the uncertainties assigned to the data being near the true standard deviations of the data. If $\hat{\kappa}$ is significantly greater than 1, the assigned uncertainties may be too large. If $\hat{\kappa}$ is significantly smaller than 1, the assigned uncertainties are too small or the assumed plate tectonic model is wrong. Thus $\hat{\kappa}$ is useful for analysing the appropriateness of the uncertainties assigned to the data. To analyse the dispersion of the data, we assigned nominal 10 km standard deviations to each magnetic-anomaly or fracture-zone crossing. We use the resulting value of $\hat{\kappa}$ from a subset of the data to infer the standard deviation of a group of data (i.e. the inferred standard deviation equals 10 km/$\hat{\kappa}^{1/2}$).

Locating edges of rigid plates

We apply a chi-square test to determine whether an increase in the misfit is significant when a new segment is added to the inverted data. We compare the sum-squared normalized misfit obtained in two ways. In the first, the data in all s segments

are inverted to obtain a best-fitting rotation and sum-squared misfit. In the second, two sums are obtained separately and then added together. These two sums are (1) the sum-squared misfit for the first $s-1$ segments, which are inverted to obtain a best-fitting rotation and sum-squared misfit, and (2) the sum-squared misfit for the sth segment, which is determined as follows. First, the crossings from the first s segments from one of the two plates are reconstructed by the finite rotation that best fits the first $s-1$ segments. The rotated crossings in the sth segment are then further rotated using one more adjustable parameter, a small rotation about a pole 90° away from the mean data location in the sth segment. For magnetic-anomaly crossings, this pole lies along the great circle connecting the mean data location and the pole of the best-fitting rotation determined from the other $s-1$ segments. For fracture-zone crossings, the pole lies along the great circle

Table 2. Fracture-zone crossings.

Latitude [°N]	Longitude [°E]	Segment #	Plate	Fracture zone	Satellite	Pass
2.13	63.61	1	af	A	Geosat ERM	asc
2.15	63.61	1	af	A	ERS-1 (35d)	asc
2.17	63.72	1	af	A	Topex	des
2.34	63.79	1	af	A	Seasat	asc
4.44	65.26	1	in	A	ERS-1 (35d)	asc
4.50	65.25	1	in	A	Seasat	des
1.75	64.42	2	af	B	ERS-1 (35d)	asc
1.80	64.50	2	af	B	ERS-1 (35d)	des
1.86	64.45	2	af	B	Geosat ERM	des
4.11	66.05	2	in	B	ERS-1 (35d)	asc
4.40	66.32	2	in	B	Seasat	asc
0.48	65.97	3	af	C	Seasat	asc
0.75	66.07	3	af	C	ERS-1 (35d)	asc
2.98	67.63	3	in	C	ERS-1 (35d)	des
3.00	67.69	3	in	C	Geosat ERM	asc
3.05	67.72	3	in	C	ERS-1 (35d)	asc
-0.05	66.25	4	af	D	ERS-1 (35d)	asc
-0.07	66.24	4	af	D	ERS-1 (35d)	des
-0.13	66.21	4	af	D	Seasat	asc
-0.27	66.03	4	af	D	Geosat ERM	asc
2.35	67.88	4	in	D	ERS-1 (35d)	asc
2.41	67.92	4	in	D	Geosat ERM	asc
-0.50	66.35	5	af	E	ERS-1 (35d)	asc
-0.52	66.36	5	af	E	Seasat	asc
-0.68	66.20	5	af	E	Geosat ERM	asc
-0.83	66.07	5	af	E	ERS-1 (35d)	des
-0.94	66.05	5	af	E	ERS-1 (35d)	des
1.72	68.01	5	in	E	ERS-1 (35d)	asc
1.84	67.99	5	in	E	ERS-1 (35d)	asc
1.87	68.11	5	in	E	ERS-1 (35d)	des
1.91	68.12	5	in	E	Geosat ERM	asc
-1.35	66.13	6	af	F	Geosat ERM	des
-1.58	66.04	6	af	F	Geosat ERM	des
0.66	67.84	6	in	F	ERS-1 (35d)	des
0.72	67.78	6	in	F	Seasat	asc
0.80	67.87	6	in	F	ERS-1 (35d)	des
0.92	67.90	6	in	F	ERS-1 (35d)	des
1.16	68.14	6	in	F	ERS-1 (35d)	asc
-3.38	66.98	7	af	Mabahiss (G2)	ERS-1 (35d)	asc
-3.40	66.95	7	af	Mabahiss (G2)	ERS-1 (35d)	des
-0.54	69.10	7	in	Mabahiss (G2)	Geosat ERM	asc
-0.63	68.99	7	in	Mabahiss (G2)	ERS-1 (35d)	des

Figure 3(b). Selected satellite-derived gravity profiles plotted along satellite ground tracks (Seasat, Geosat/ERM, ERS1 ascending passes, and Topex/Poseidon descending passes only) in the same oblique Mercator projection as in (a). These profiles have ground tracks that are the most perpendicular to the strikes of the younger portion of the fracture zones. Negative values are shaded and projected to the right of the figure (not perpendicular to tracks). Dashed lines show interpreted fracture-zone traces, which are based not only on the data shown but on additional profiles as well. Small open circles are gravity troughs. For our plate-motion inversion, we selected only those troughs near anomaly 5.

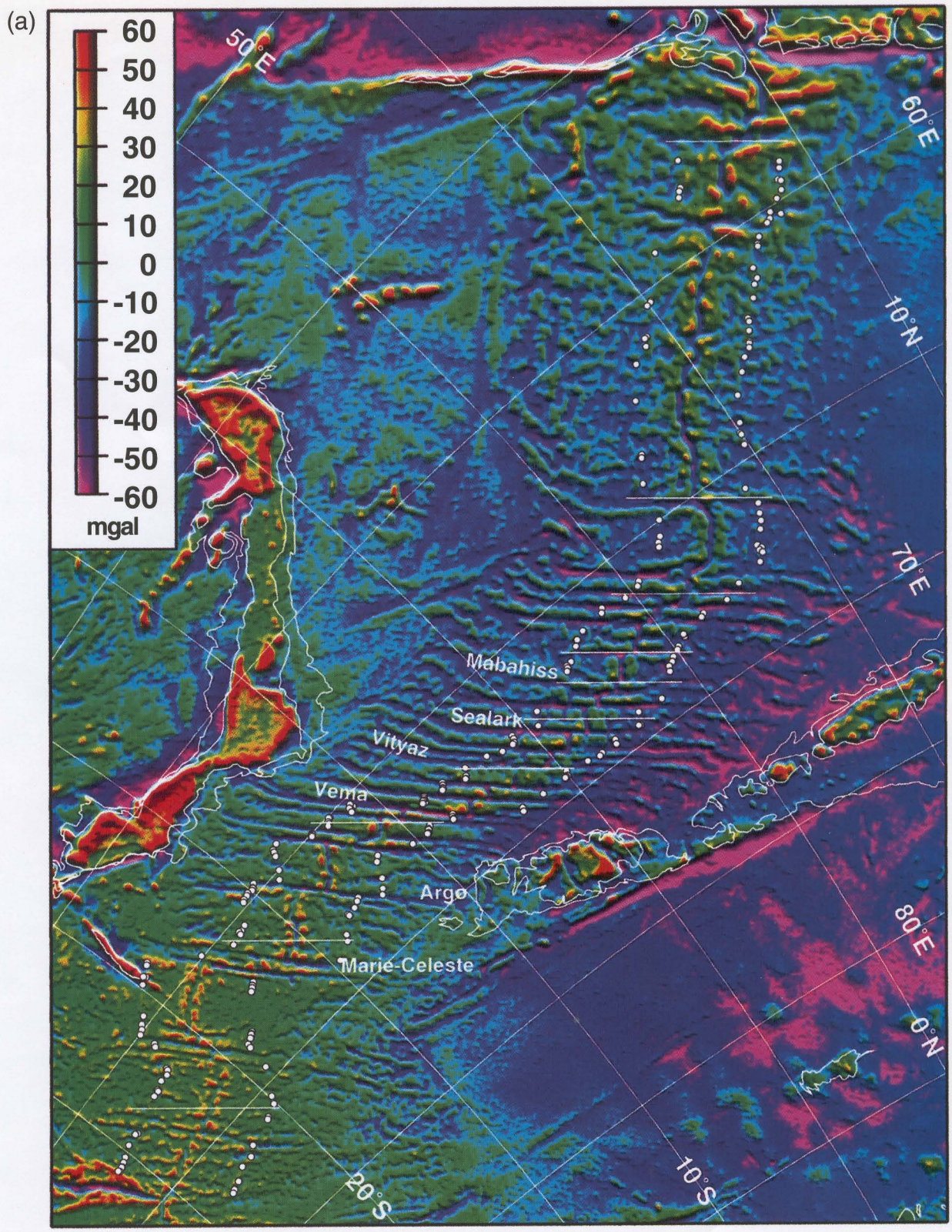

Figure 3(a). Crossings of anomaly 5 (white circles outlined in black) and gridded satellite-derived gravity (Smith & Sandwell 1995) are shown in an oblique Mercator projection about the Euler pole (24.13°N, 30.37°E) for the rotation of India relative to Africa since chron 5. Small circles about this pole of rotation are horizontal lines in this projection. Some horizontal white lines are shown for reference. Artificial illumination from the top right of the figure enhances the gravity signature of the fracture zones. Names of six fracture zones are shown just above the fracture-zone trough. North of ~5°S the gravity troughs are aligned along fracture zones that appear horizontal in this projection. South of ~5°S the fracture-zone trends progressively depart from small circles about the India–Africa Euler pole.

Table 2. (*Continued.*)

-0.83	68.95	7	in	Mabahiss (G2)	ERS-1 (35d)	des
-3.84	67.45	8	af	H	Geosat ERM	asc
-3.85	67.37	8	af	H	Topex	asc
-4.08	67.28	8	af	H	Topex	asc
-4.13	67.15	8	af	H	ERS-1 (35d)	asc
-1.22	69.58	8	in	H	ERS-1 (35d)	des
-1.38	69.43	8	in	H	Geosat ERM	asc
-1.40	69.42	8	in	H	ERS-1 (35d)	asc
-4.90	67.67	9	af	Sealark (I)	Geosat ERM	des
-5.01	67.63	9	af	Sealark (I)	Geosat ERM	des
-5.13	67.37	9	af	Sealark (I)	ERS-1 (35d)	asc
-5.18	67.27	9	af	Sealark (I)	ERS-1 (35d)	des
-2.44	69.65	9	in	Sealark (I)	ERS-1 (35d)	asc
-2.99	69.19	9	in	Sealark (I)	ERS-1 (35d)	des
-3.02	69.27	9	in	Sealark (I)	Seasat	asc
-5.79	67.51	10	af	J	ERS-1 (35d)	asc
-6.04	67.21	10	af	J	Geosat ERM	des
-6.18	67.16	10	af	J	Geosat ERM	des
-6.19	67.18	10	af	J	Seasat	asc
-3.47	69.44	10	in	J	Seasat	asc
-6.75	67.40	11	af	Vityaz (K)	Seasat	asc
-6.91	67.20	11	af	Vityaz (K)	Geosat ERM	asc
-7.02	67.07	11	af	Vityaz (K)	ERS-1 (35d)	asc
-7.09	67.03	11	af	Vityaz (K)	Topex	des
-7.29	66.81	11	af	Vityaz (K)	ERS-1 (35d)	des
-4.51	69.38	11	in/au	Vityaz (K)	ERS-1 (35d)	asc
-4.51	69.30	11	in/au	Vityaz (K)	Geosat ERM	des
-4.53	69.21	11	in/au	Vityaz (K)	Geosat ERM	asc
-4.93	69.13	11	in/au	Vityaz (K)	Geosat ERM	des
-4.93	69.09	11	in/au	Vityaz (K)	Topex	des
-7.60	67.48	12	af	L	Geosat ERM	asc
-7.66	67.44	12	af	L	ERS-1 (35d)	des
-7.77	67.28	12	af	L	Topex	des
-7.80	67.24	12	af	L	ERS-1 (35d)	asc
-5.36	69.66	12	in/au	L	Topex	asc
-5.41	69.58	12	in/au	L	ERS-1 (35d)	asc
-5.43	69.56	12	in/au	L	Geosat ERM	asc
-5.60	69.34	12	in/au	L	ERS-1 (35d)	des
-5.63	69.34	12	in/au	L	Topex	des
-8.43	67.27	13	af	M	ERS-1 (35d)	des
-8.72	66.93	13	af	M	Seasat	asc
-8.73	66.86	13	af	M	Seasat	asc
-8.85	66.75	13	af	M	ERS-1 (35d)	asc
-8.85	66.81	13	af	M	Seasat	asc
-6.13	69.52	13	in/au	M	Topex	des
-6.22	69.35	13	in/au	M	Topex	asc
-6.34	69.31	13	in/au	M	Seasat	des
-6.36	69.17	13	in/au	M	ERS-1 (35d)	des
-6.44	69.27	13	in/au	M	Topex	asc
-6.54	69.12	13	in/au	M	ERS-1 (35d)	asc
-6.60	69.11	13	in/au	M	ERS-1 (35d)	des
-11.06	65.51	14	af	O	Seasat	asc
-11.25	65.10	14	af	O	Geosat ERM	des

Table 2. (*Continued.*)

-11.25	65.14	14	af	O	ERS-1 (35d)	asc
-11.28	65.19	14	af	O	ERS-1 (35d)	des
-8.88	68.00	14	au	O	Geosat ERM	asc
-8.89	67.84	14	au	O	Seasat	des
-8.99	67.86	14	au	O	ERS-1 (35d)	des
-9.12	67.78	14	au	O	Topex	des
-9.23	67.71	14	au	O	Seasat	des
-9.31	67.58	14	au	O	ERS-1 (35d)	asc
-11.89	65.28	15	af	P	ERS-1 (35d)	asc
-12.16	64.99	15	af	P	ERS-1 (35d)	des
-12.17	64.92	15	af	P	Geosat ERM	asc
-9.69	67.96	15	au	P	Seasat	des
-9.69	68.08	15	au	P	Topex	asc
-9.70	67.99	15	au	P	Topex	des
-10.00	67.73	15	au	P	ERS-1 (35d)	asc
-10.08	67.62	15	au	P	ERS-1 (35d)	des
-14.31	65.31	16	af	Argo (R)	Geosat ERM	des
-14.36	65.21	16	af	Argo (R)	ERS-1 (35d)	des
-14.44	65.14	16	af	Argo (R)	ERS-1 (35d)	asc
-14.48	65.18	16	af	Argo (R)	ERS-1 (35d)	des
-14.51	65.23	16	af	Argo (R)	Geosat ERM	des
-14.64	64.95	16	af	Argo (R)	Seasat	asc
-12.12	68.32	16	au	Argo (R)	Seasat	asc
-12.13	68.25	16	au	Argo (R)	Seasat	asc
-12.20	68.23	16	au	Argo (R)	ERS-1 (35d)	asc
-12.25	68.20	16	au	Argo (R)	Seasat	asc
-12.42	67.97	16	au	Argo (R)	Geosat ERM	asc
-12.64	67.76	16	au	Argo (R)	ERS-1 (35d)	des
-12.71	67.72	16	au	Argo (R)	Seasat	des
-12.76	67.63	16	au	Argo (R)	ERS-1 (35d)	asc
-12.78	67.73	16	au	Argo (R)	ERS-1 (35d)	des
-16.44	65.61	17	af	R3	ERS-1 (35d)	asc
-16.57	65.44	17	af	R3	Topex	asc
-16.60	65.41	17	af	R3	ERS-1 (35d)	des
-16.67	65.33	17	af	R3	Geosat ERM	asc
-16.67	65.39	17	af	R3	ERS-1 (35d)	des
-14.23	68.73	17	au	R3	Geosat ERM	asc
-14.25	68.69	17	au	R3	ERS-1 (35d)	asc
-14.49	68.42	17	au	R3	Seasat	des
-17.03	65.75	18	af	S	ERS-1 (35d)	asc
-17.17	65.55	18	af	S	Geosat ERM	asc
-17.17	65.57	18	af	S	Geosat ERM	des
-17.35	65.27	18	af	S	Topex	des
-17.35	65.24	18	af	S	ERS-1 (35d)	des
-17.42	65.12	18	af	S	ERS-1 (35d)	asc
-17.43	65.10	18	af	S	Topex	asc
-15.00	68.87	18	au	S	ERS-1 (35d)	asc
-15.02	68.89	18	au	S	Topex	asc
-15.16	68.62	18	au	S	ERS-1 (35d)	des
-15.45	68.25	18	au	S	ERS-1 (35d)	asc
-21.27	65.48	19	af	V	Seasat	des
-21.37	65.34	19	af	V	ERS-1 (35d)	asc
-21.41	65.19	19	af	V	Geosat ERM	des

Table 2. (*Continued.*)

-19.00	69.29	19	au	V	Geosat ERM	asc
-19.08	69.14	19	au	V	ERS-1 (35d)	des
-19.08	69.17	19	au	V	Geosat ERM	des
-19.13	69.12	19	au	V	ERS-1 (35d)	asc
-19.22	69.11	19	au	V	ERS-1 (35d)	des
-19.30	68.90	19	au	V	Topex	des
-21.15	66.39	20	af	W	Topex	asc
-21.31	66.13	20	af	W	Seasat	asc
-21.35	66.06	20	af	W	ERS-1 (35d)	asc
-21.43	65.95	20	af	W	Geosat ERM	asc
-19.05	69.86	20	au	W	ERS-1 (35d)	des
-19.09	69.82	20	au	W	ERS-1 (35d)	asc
-19.36	69.45	20	au	W	Geosat ERM	asc
-23.54	67.34	21	af	Y	ERS-1 (35d)	des
-23.61	67.33	21	af	Y	ERS-1 (35d)	asc
-23.69	67.30	21	af	Y	ERS-1 (35d)	des
-23.72	67.23	21	af	Y	Seasat	asc
-23.72	67.08	21	af	Y	Geosat ERM	des
-23.75	67.01	21	af	Y	Geosat ERM	asc
-21.19	71.19	21	au	Y	Geosat ERM	des
-21.34	71.08	21	au	Y	ERS-1 (35d)	asc
-21.38	71.10	21	au	Y	Geosat ERM	des
-21.62	71.40	22	au	Y1	ERS-1 (35d)	des
-21.82	71.20	22	au	Y1	ERS-1 (35d)	asc
-21.86	71.15	22	au	Y1	Seasat	des
-24.11	67.41	22	af	Y1	Seasat	asc
-24.11	67.45	22	af	Y1	ERS-1 (35d)	asc
-24.22	67.22	22	af	Y1	Geosat ERM	asc
-24.30	67.15	22	af	Y1	ERS-1 (35d)	des

Each crossing is a gravity trough along a satellite profile. The crossings are sorted by palaeotransform segment and plate (af = African, in = Indian, au = Australian). Abbreviations: 35d, ERS-1 35 day cycle; Geosat ERM, Geosat Exact Repeat Mission; asc, ascending pass; des, descending pass.

perpendicular to that for magnetic-anomaly crossings. These two poles of incremental rotation are single-segment analogues to the poles of rotation used for the magnetic-anomaly and fracture-zone 'partial uncertainty rotations' of Stock & Molnar (1983) and Molnar & Stock (1985).

The same data are thus used in each model, with the second model having one more adjustable parameter, and hence one less degree of freedom, than the first. If the errors are normally distributed, and if departures from the best-fitting rotation are small, then the difference in the normalized sum-squared misfit for the two models is expected to be chi-square distributed with one degree of freedom. Because we make this test many times, more than 50, in each experiment, the usual confidence level of 95 per cent, corresponding to a significance level of 5 per cent, is too weak because the chances of a false reading are high. Even a confidence level of 99 per cent is too weak because the test is repeated more than 50 times. The appropriate level of confidence is about 99.9 per cent, corresponding to a significance level of 0.1 per cent, which is approximately one-fiftieth of 5 per cent (Fig. 5). Starting our inversions with two segments, the bare minimum needed for convergence, we add one segment at a time to the prior subset until we reach 54, the total number of segments.

RESULTS

Fracture zones

The new altimetric data permit the delineation of all fracture zones, as well as some wandering offsets and other fine-scale features. The pattern of magnetic anomalies and fracture zones shows that the Central Indian and Carlsberg ridges were almost as segmented at chron 5 as now, suggesting that the complex fracture-zone pattern has been stable since at least 11 Ma. It may have changed little since the Late Eocene (Fig. 1). Whereas most of the Carlsberg Ridge appears as a long and continuous spreading axis, the Central Indian and southern Carlsberg ridges are offset by many fracture zones, few of which have been named. For practical purposes, we label the major fracture zones from A to Z, with some additional fracture zones labelled as a, b, and c, and F1, G1, etc. (Fig. 1).

From 10°N (Owen fracture zone) to 2°N (fracture zone C), the present Carlsberg Ridge is nearly continuous, with about 1400 km of spreading segments versus 275 km of transform segments. From 2°N to 13°S (fracture zone Q) inclusive, the ridge has 16 offsets excluding the small offsets at F1 and G1.

On average, the ridge segments are shorter than the transform segments (1015 km of ridge segments versus 1215 km of transform segments including fracture zones C and Q). The narrowness of the corridors (63 km on average) thus makes the interpretation of magnetic profiles difficult when the profiles fail to be nearly parallel to the fracture zones. South of 13°S, the corridors become wider (1500 km versus 690 km along transform fault segments). The southernmost major offset occurs along the Marie-Celeste fracture zone (fracture zone T). The sense of ridge offset along fracture zones is uniformly right-lateral from the Owen triple junction to the Marie-Celeste fracture zone (Figs 1 and 3a). South of the Marie-Celeste fracture zone to 21°S, four successive fracture zones—U, V, W, and W1—have left-lateral offsets (Fig. 1). South of these four fracture zones, the ridge offsets are again uniformly right-lateral. The region where the ridge is highly segmented corresponds to an intermediate-wavelength gravity low, whereas the long ridge segments along the Carlsberg Ridge and southern Central Indian Ridge are located on regional gravity highs.

Dashed lines in Fig. 1 outline the lineated and continuous gravity lows that reflect the tectonic fabric. For transform faults with offsets greater than ~40 km, the fracture zones tend to be continuous and their expression is symmetric on the conjugate plate. The two exceptions, the Vema (N) and Q fracture zones, are more continuous on the African plate than on the conjugate plate. Where the present transform offset is smaller than ~30 km, the fracture zones are discontinuous and their shape in many places fails to mirror the conjugate corridors (e.g. F1, R1, R3, Y1, Y2, Y3). The origin of these lineated gravity lows is unclear, but they clearly fail to follow flow-lines. If any one records the trace of an ancient transform fault, it is a transform fault that has migrated relative to other transform faults and presumably relative to the plate interior. Several V- or U-shaped lineaments, symmetric about the present ridge axis, are also observed and probably represent conjugate pseudo-faults associated with propagating rifts, some of which are slow propagators or wandering offsets (*cf.* Atwater 1989). The best example of a wandering offset is Q1, which records alternating southward and northward propagation of overlap of the Q–Q1 ridge segment with the Q1–R ridge segment. Some of them, including G1, G2, and U, are flow-line fracture zones in their younger portions, indicating that their migration ceased millions of years ago.

There are 32 palaeotransform faults and five non-transform offsets that appear to be wandering offsets along the Central Indian and Carlsberg ridges at chron 5. The distance between palaeotransform faults along the Carlsberg Ridge at chron 5 is 200 km (mean), with half the distances being between 34 and 101 and the other half being between 195 and 724 km. The mean distance between fracture zones along the Central Indian Ridge is 96 km (mean), with half between 30 and 59 km and half between 59 and 347 km. The offset of anomaly 5 can be estimated for 29 of these palaeotransform faults and non-transform offsets. Seven of the 29 offsets are 28 km or less, with the shortest offset (19 km) being along fracture zone Y1, 17 have offsets between 38 and 85 km (along the Sealark fracture zone), and the longest five range from 96 (along the Argo fracture zone) to 255 km (along the Vema fracture zone).

Analysis of dispersion

To improve our understanding of the uncertainties in the locations of magnetic-anomaly and fracture-zone crossings, we examined the dispersions of subsets of the data inverted to find best-fitting rotations. Guided by a preliminary analysis of the limits of the rigid Indian plate and of the limits of the rigid Australian plate, the data were further divided into three subsets: (1) those data thought to record motion between the Indian and African plates; (2) those data thought to record motion between the Australian and African plates; and (3) those data suspected of recording neither one. In the analysis of dispersion only those data thought to record motion between rigid plates were used.

All data

When all data except those in the deforming zone are given equal weight, the standard deviation of the Africa–India crossings is 4.0 ± 0.6 km with 83 degrees of freedom. (In this section uncertainties following '$\pm$' signs are 95 per cent confidence limits.) The standard deviation for the Africa–Australia crossings is 4.0 ± 0.5 km with 127 degrees of freedom.

Magnetic-anomaly crossings

Inversion of the magnetic-anomaly crossings with no fracture-zone crossings gave best-fitting rotations similar to those found when the fracture-zone crossings were included. It thus seems reasonable to expect that the asymptotic approximations made by Chang (1988) are satisfied when fracture-zone data are excluded and consequently that the estimates of statistical parameters are valid. We found that the standard deviation of the Africa–India magnetic-anomaly crossings is 3.1 ± 0.7 km with 41 degrees of freedom. The standard deviation of the Africa–Australia magnetic-anomaly crossings is 4.0 ± 0.7 km with 61 degrees of freedom. Although the confidence limits overlap, an F-ratio test indicates that the dispersion of the Africa–Australia magnetic anomaly crossings is significantly greater than that of the Africa–India crossings, but only marginally so (i.e. at the 4.4 per cent significance or 95.6 per cent confidence level). If we add the Russian crossings to the Africa–India data, the standard deviation increases to 4.0 ± 0.7 km with 60 degrees of freedom, which is consistent with the dispersion of the Africa–Australia data.

Fracture-zone crossings

Inversion of the Africa–India fracture-zone crossings with no magnetic-anomaly crossings gave a best-fitting rotation having a magnitude several times larger than that found when the magnetic-anomaly crossings were also included. Thus, the dispersion results must be treated with caution because the asymptotic approximations may be poor and thus the true dispersions may be significantly larger than estimated. The standard deviation of the Africa–India crossings is 4.3 ± 0.9 km with 39 degrees of freedom. For the Africa–Australia fracture-zone crossings, the magnitude of the rotation is about twice that obtained when the magnetic-anomaly crossings are also included. Again, caution is required in interpreting the results. We find that the standard deviation of the Africa–Australia crossings is 3.8 ± 0.7 km with 63 degrees of freedom, which differs insignificantly from that for Africa–India.

Therefore, when the data are not separated into categories based on preconceived notions about relative accuracy, the standard deviations of the locations of the crossings are near

4 km, except for the Africa–India magnetic crossings (excluding the Russian crossings), which have smaller standard deviations.

Smaller subsets of data

Inversions of smaller subsets of the data were used to assess the dispersion of each category (A, B, C, and D) of magnetic-anomaly crossing. The crossings were too sparse to give more than a few meaningful estimates of dispersion for a single category of data. Instead, we rely on combinations of two or three categories of data to obtain a reliable estimate of dispersion. The results demonstrate neither consistency nor inconsistency with our belief that the A data are more accurate than the B, the B more accurate than the C, etc. For example, when the A and B Africa–India magnetic crossings are combined, the standard deviation of the crossings is 3.3 ± 1.4 km with 11 degrees of freedom. When the B, C, and D data are combined, the standard deviation is 3.6 ± 1.1 km with 21 degrees of freedom, and when the C and D crossings are combined, the standard deviation of the crossings is 3.8 ± 1.5 km with 12 degrees of freedom. These three estimates form a neat sequence, but with clearly overlapping confidence intervals. When the A, B, and C data are combined, however, the standard deviation is 2.9 ± 1.0 km with 18 degrees of freedom, smaller than either the A plus B or B plus C combination, but insignificantly so. The D data alone are too sparse to estimate their standard deviation. However, if the Russian data are included as D data, as they were in our preliminary but not our final analysis, their standard deviation is 5.2 ± 1.6 km with 20 degrees of freedom. From the A data we can obtain a tentative estimate of standard deviation of 2.5 ± 1.3 km with only seven degrees of freedom.

When the A and B Africa–Australia magnetic crossings are combined, the standard deviation is 3.2 ± 1.0 km with 22 degrees of freedom. When the A, B, and C crossings are combined, the standard deviation is 3.1 ± 0.6 km with 46 degrees of freedom. The B and C data give 2.7 ± 0.8 km with 21 degrees of freedom. The B, C, and D data give a standard deviation of 3.1 ± 0.7 km with 36 degrees of freedom, and the C and D data give a standard deviation of 3.2 ± 1.0 km with 19 degrees of freedom. In light of the 4.0 ± 0.7 km standard deviation of all Africa–Australia crossings, these dispersions are surprisingly small and hint that the A and D data are somewhat inconsistent with one another. From the A data we estimate a tentative standard deviation of 3.4 ± 1.8 km with only seven degrees of freedom.

Error budget

From this dispersion analysis and our preconceived ideas about the relative uncertainties of the data, we assign 1σ uncertainties of 3.0, 3.2, 3.9, and 5.2 km, respectively, to the A, B, C, and D data. The 3.0 km error may seem conservative for those cruises and flights with GPS navigation, but this seems to us to be the smallest error warranted by the dispersion analysis. Moreover, many 'A' data, including those from the 1990 aeromagnetic survey, were not merged with GPS navigation. The estimates for the B and C categories are not inconsistent with the accuracy of the Transit satellite system, thought to be about ± 1 nautical mile (i.e. ± 1.85 km). The error on the D data is based in part on the standard deviation determined from data including the Russian data, and may overestimate the errors in the rest of the D data. If we invert all the magnetic anomaly crossings with this error budget, $\hat{\kappa}$ is 1.609 with a 95 per cent confidence interval from 0.989 to 2.376 with 41 degrees of freedom for the India–Africa data. This value of $\hat{\kappa}$ indicates that on average the crossings are dispersed only about 0.79 times as much as expected from the errors that we assigned. $\hat{\kappa}$ is 0.866 with a 95 per cent confidence interval from 0.587 to 1.199 with 61 degrees of freedom for the Australia–Africa data. This value of $\hat{\kappa}$ indicates that on average the standard deviation of the crossings is only about 7 per cent greater than expected from the errors that we assigned. In the aggregate, the distribution of normalized residuals of magnetic-anomaly crossings have larger kurtosis than expected for a Gaussian distribution; that is, the central peak is sharper and there are a few more observations with large misfits than expected for a Gaussian distribution (upper left corner of Fig. 7). It is unclear whether this is caused by the existence of a few large outliers, by a real difference in dispersion of Africa–India versus Africa–Australia crossings, or some other explanation.

For both the Africa–India and Africa–Australia data sets, $\hat{\kappa}$ differs insignificantly from one. However, the ratio $\hat{\kappa}_{\text{af-in}}/\hat{\kappa}_{\text{af-au}}$ differs significantly from one at the 2 per cent significance level. Therefore, without further adjustment, the confidence limits tend to overestimate the errors for the India–Africa rotation by a factor of about 1.36 relative to the errors for the Australia–Africa rotation. Thus, this difference is likely to be one of the causes, if not the only cause, of the large kurtosis of the residuals. We know of no compelling reason, however, why the Africa–Australia magnetic-anomaly crossings should be more dispersed than the Africa–India crossings. Hereinafter we use the assigned errors without any further correction. We do so because the dispersion of the Africa–Australia data differs negligibly from the assigned errors, and because the assigned errors are likely to be as large or larger than the true errors for the Africa–India data, thus giving us a conservative estimate of the latter uncertainties.

Summary

In summary, the 1σ uncertainties that we assign to magnetic-anomaly crossings range from 3.0 to 5.2 km. The corresponding 95 per cent confidence limits range from 5.9 to 10.2 km. The Africa–Australia anomaly crossings are about 7 per cent more dispersed and the Africa–India crossings about 21 per cent less dispersed than expected from the assigned errors. These errors are slightly smaller than errors assigned by prior workers, who assigned uncertainties with typical values of 10 to 15 km (e.g. Stock & Molnar 1988; Royer & Chang 1991). Thus the results suggest that prior uncertainties were too pessimistic, but only by about a factor of 2.

For the fracture zones, given the reservations mentioned earlier, we choose to be more conservative than suggested by the dispersion analysis and assign a standard error of 5.0 km to all fracture-zone crossings. Our aim is for this larger error to allow for the gravity troughs to be located up to 5 to 10 km from the actual location of the palaeotransform. If there is a systematic offset of the gravity trough from the palaeotransform fault, the rotation uncertainties may be underestimated in this component because so many fracture-zone crossings are used. Fortunately, any such effect must be subtle as enlarged plots of the fit of the fracture-zone crossings reveal no obvious pattern of consistent misfit.

Evidence for a system of three rigid plates

Fig. 4 illustrates the size of the misfit if India and Australia are wrongly assumed to be part of a single rigid Indo–Australian plate. If the Indo–Australian magnetic-anomaly and fracture-zone crossings are reconstructed using the rotation that best fits roughly the northern 35 per cent of the data (left side of Fig. 4) or the southern 45 per cent of the data (right side of Fig. 4), data at the opposite end of the ridge system are poorly fit with gaps up to 90–100 km. This ability to fit significant subsets of data on either end of the Carlsberg and Central Indian ridges is consistent with the existence of a set of three rigid plates and hence of a plate boundary in addition to the two systems of spreading ridges. The high level of

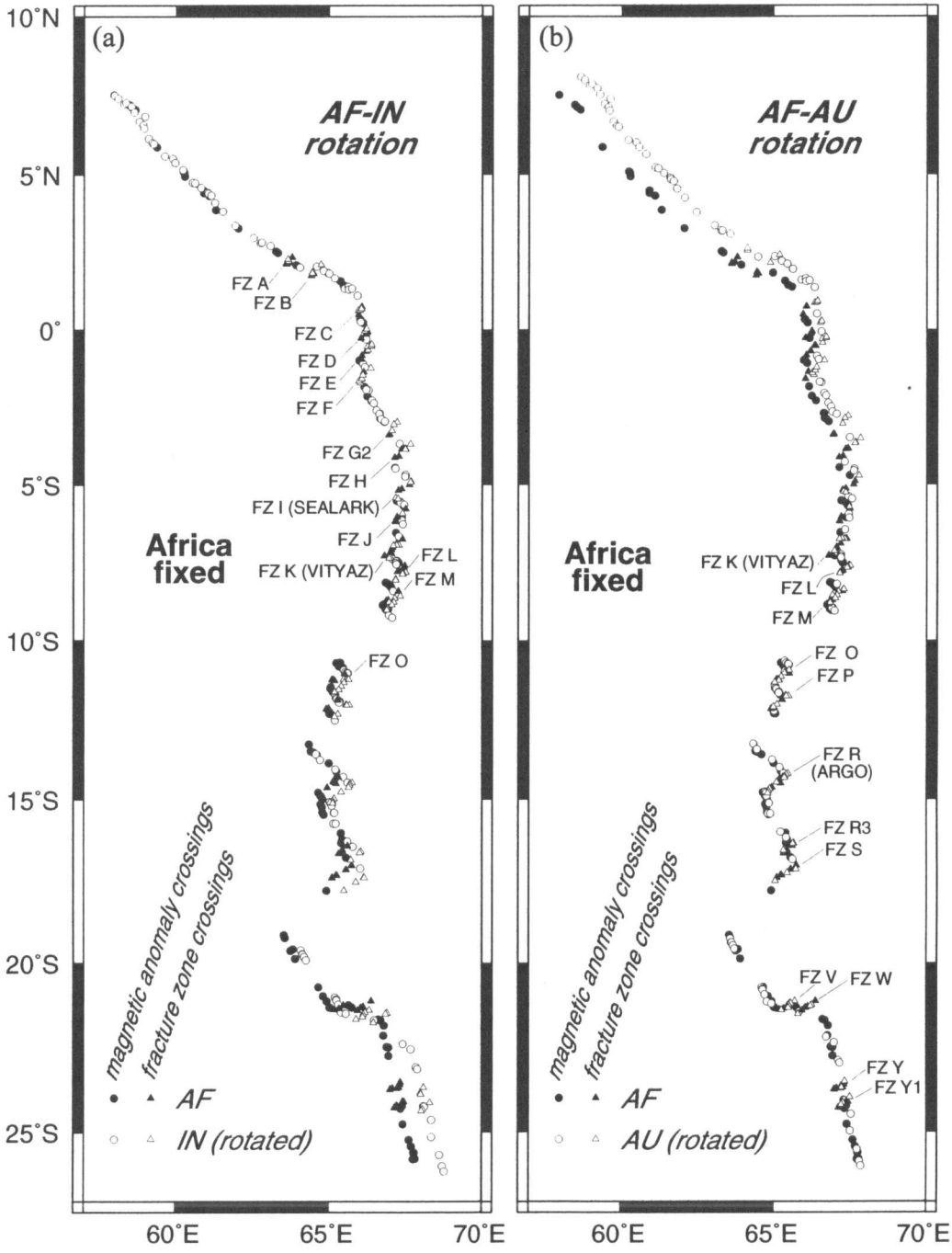

Figure 4. Chron 5 reconstructions using (a) the best-fitting rotation of the Indian plate to the African plate and (b) the best-fitting rotation of the Australian plate to the African plate. In (a), data north of ~5°S are well fit, consistent with them recording the motion between rigid or nearly rigid Indian and African plates; data are increasingly misfit with increasing distance south of 5°S, with the southernmost data being misfit by ~90 km. In (b), data south of ~10°S are well fit, consistent with them recording the motion between rigid or nearly rigid Australian and African plates; data are increasingly misfit with increasing distance north of 11°S, with the northwesternmost data being misfit by 90–100 km. The goodnesses of fit of these two separate reconstructions for data north of ~5°S and south of 10°S are consistent with a model in which India, Africa, and Australia are treated as three distinct rigid or nearly rigid plates.

seismicity and the deformation pattern in the Central Indian Basin show that the additional plate boundary is between the Indian and Australian plates, rather than within the African plate. (Here we follow the convention used in global plate-motion model NUVEL-1 of treating Africa as a single rigid plate. It can reasonably be considered to be two plates, a western Nubian plate and an eastern Somalian plate. Herein, what is referred to as the African plate could equally well be referred to as the Somalian plate.)

Figs 3(a) and (b) are oblique Mercator projections about the best-fitting chron 5 Africa–India Euler pole (discussed below). On such a projection, the portions of the fracture zones created since chron 5 should align along small circles centred on the Euler pole; in this projection these small circles are horizontal and parallel straight lines. Southwards from the Vityaz fracture zone there is a subtle and increasing depature from the horizontal of the young portions of the fracture zones, which becomes obvious south of and including the Vema fracture zone. These departures show that the southern fracture zones record motion different from that recorded north of the Vityaz fracture zone.

The edges of the rigid Indian and Australian plates

Analysis of present plate motions (i.e. the average since chron 2A, about 3 Ma) suggests that the boundary between the Indian and Australian plates intersects the Central Indian Ridge near or just north of ~9°S, near the northeastern end of the Vema transform fault. The data available for present plate motions are inadequate to determine whether the boundary is wide or narrow where it intersects the Central Indian Ridge (DeMets *et al.* 1994a). Off-ridge seismicity occurs east of the Central Indian Ridge between about 3°S and 8°S, that is, between the J and Vema (N) fracture zones. If significant deformation has occurred throughout this region, then the Indo–Australian seafloor between these two fracture zones has moved neither as part of the rigid Indian plate nor as part of the rigid Australian plate. Either possibility can be tested by inverting the data in question with those data believed to record motion of one of these two plate pairs. To investigate this further, we progressively inverted larger subsets of our data starting in one case from the Owen fracture zone (and triple junction) and in the other case from the Rodrigues (Indian Ocean) triple junction (Fig. 5).

In the analysis that progresses eastwards and southwards from Owen triple junction, the first significant misfit occurs with the addition of the crossings of fracture zone L (the fracture zone immediately south of the Vityaz fracture zone). This indicates that the Indo–Australian seafloor near fracture zone L has moved significantly relative to the Indian plate. Therefore the edge of the rigid Indian plate lies northwest of fracture zone L. Although not misfit significantly, the magnetic-anomaly crossings between the Vityaz fracture zone and fracture zone L, as well as the crossings of the Vityaz fracture zone itself, are not well fit as part of the rigid Indian plate. Thus we suspect, but cannot demonstrate, that the edge of the rigid Indian plate along the Central Indian Ridge lies somewhere northwest of the Vityaz fracture zone.

Progressing northwards from the Rodrigues triple junction, the first significant misfit occurs with the addition of the anomaly crossings from the ridge segment northwest of fracture zone O and southeast of the Vema (N) fracture zone. Because the fracture-zone crossings of fracture zone O and all data south of fracture zone O, in particular the magnetic-anomaly crossings along the ridge immediately southeast of it, are fit satisfactorily, we believe that significant motion has been occurring on the 'inactive' portion of fracture zone O on the Indo–Australian side of the spreading ridge and that this is the northwestern limit of the rigid Australian plate. Thus the northern edge of the Australian plate may be more sharply localized than is the southern edge of the Indian plate along the Central Indian Ridge. The misfit of anomaly 5 north of fracture zone O is not inconsistent with the result from anomaly 2A, for which the data lack the power to distinguish between a narrow boundary located a little farther north, near the Veam fracture zone, and a wider boundary that could include the ridge north of fracture zone O, as well as a much larger region.

Thus, the data from the Rodrigues triple junction to, and including, fracture zone O record the motion between the Australian and African plates. For these segments, the seafloor on the Australian side of the Central Indian Ridge is part of the rigid Australian plate. The data from the Owen fracture zone through the ridge segment between fracture zone L and the Vityaz (K) fracture zone are satisfactorily fit by a model of separating rigid African and Indian plates, whereas fracture zone L is misfit significantly. Within the uncertainties, the seafloor northeast of these segments could be part of the rigid Indian plate, which must end somewhere northwest of fracture zone L. We suspect that it ends northwest of the Vityaz fracture zone. Therefore, in the analysis below we use data between the Owen fracture zone and fracture zone J, including fracture zone J, which is between the Sealark and Vityaz fracture zones, to estimate the rotation between the Indian and African plates, while excluding data farther southeast.

Plate rotations

After data are excluded between fracture zones J and O, 308 crossings (146 fracture-zone crossings and 162 magnetic-anomaly crossings) of the 377 total crossings (excluding the 19 Russian magnetic-anomaly crossings) remain. The Africa–India rotation is determined from the inversion of 132 data (70 magnetic-anomaly crossings and 62 fracture-zone crossings) divided into 23 segments. The Africa–Australia rotation is determined from 176 data (92 magnetic-anomaly crossings and 84 fracture-zone crossings) divided into 23 segments. The best-fitting rotations (Fig. 6, Table 3) are qualitatively similar to those of Royer & Chang (1991), but the uncertainty regions shrink greatly. Royer & Chang's best-fitting rotations lie outside the new compact 95 per cent confidence regions. The volume of the uncertainty region shrinks by a factor of 98 for the Africa–India rotation and by a factor of 78 for the Africa–Australia rotation. We can now directly resolve the motion between the African and Australian plates, whereas Royer & Chang (1991) had to use closure of the Africa–Antarctica–Australia plate-motion circuit to overcome the paucity of data along the Central Indian Ridge. For both finite rotations, the residual distance between each inverted datum and the corresponding great-circle segment (i.e. the misfit of each data point) never exceeds 2.2 times the assigned 1σ error for any category of data (A, B, C, D, or fracture zone; Fig. 7). The $\hat{\kappa}$ values for both determinations (Table 3) are slightly greater than one. At first glance this suggests that the assigned errors are on average slightly overestimated and could be reduced by a factor of

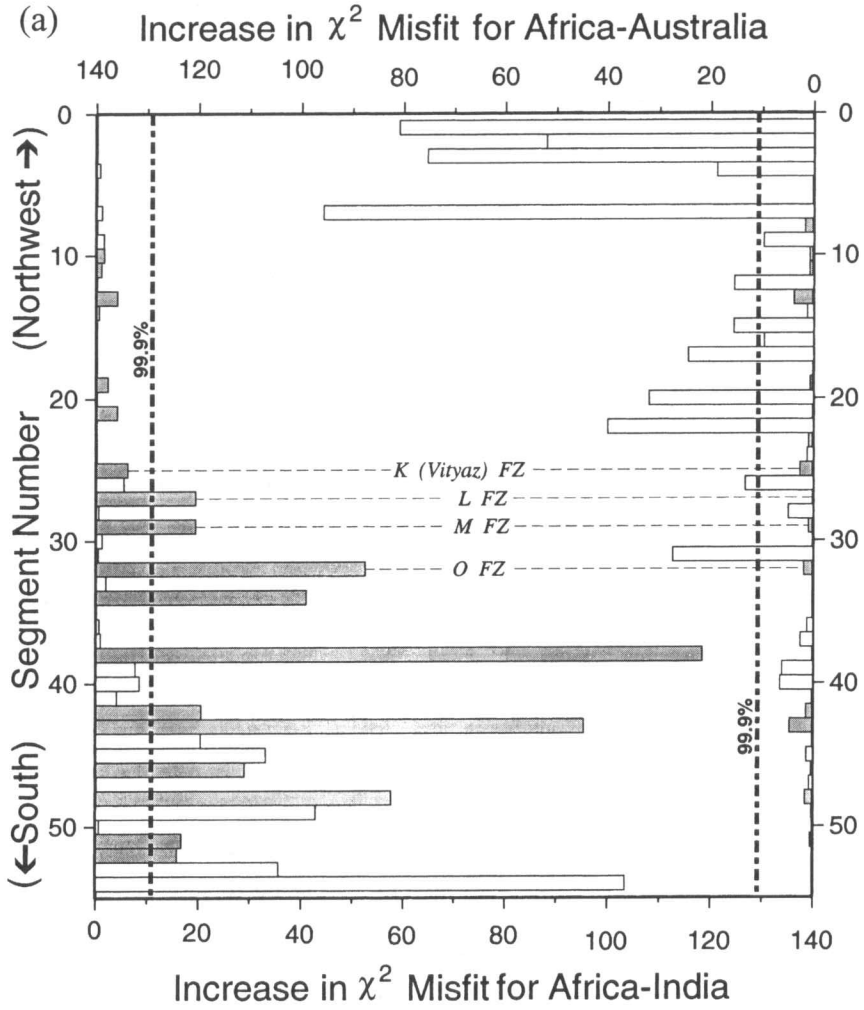

Figure 5. Test of whether a plate-boundary segment is consistent with having recorded motion between the same pair of rigid plates as other data. Results shown along the left edge of the figure are tests of whether segments are consistent with recording the motion between the Indian and African plates. Results shown along the right edge of the figure are tests of whether segments are consistent with recording the motion between the Australian and African plates. A plate segment consists either entirely of magnetic-anomaly crossings or entirely of fracture-zone crossings. Results from magnetic-anomaly segments are shown by open bars and those from fracture-zone segments by stippled bars. In part (a), the data are used to place bounds on the location of the edges of the rigid Indian or rigid Australian plate. Each test for Africa–India assumes that all data on segments north or northwest of the segment in question record Africa–India motion. Each test for Africa–Australia assumes that all data on segments south of the segment in question record Africa–Australia motion. The results indicate that fracture zone L (the unnamed fracture zone immediately south of the Vityaz fracture zone) is misfit significantly when assumed to record motion between the Indian and African plates. Thus the southern limit of the rigid Indian plate lies north of fracture zone L. The results further indicate that magnetic-anomaly crossings south of the Vema fracture zone and north of fracture zone O (the unnamed fracture zone immediately south of the Vema) are misfit significantly when assumed to record motion between the Australian and African plates. Thus the northern limit of the rigid Australian plate lies south of this ridge segment, possibly along fracture zone O. In part (b), data north and northwest of (but excluding) fracture zone K are assumed to record Africa–India motion, whereas data south of fracture zone O inclusive are assumed to record Africa–Australia motion. Thus, part (b) better illustrates the poor agreement of segments far beyond the edge of either rigid plate.

about 0.9 ($=1/\hat{\kappa}^{1/2}$). We make no such reduction because the uncertainties in the fracture-zone crossings were intentionally overestimated relative to their dispersion in the hope that this might partially compensate for any systematic errors introduced by the use of satellite altimetry data.

Fig. 6 also shows that the poles of rotation for chron 5 are similar to those for chron 2A (DeMets *et al.* 1994a), but the chron 2A Africa–Australia pole lies east of and differs significantly from the chron 5 pole. The rates of rotation averaged over the past 11 Myr, 0.401° Myr^{-1} for Africa–India and 0.575° Myr^{-1} for Africa–Australia, are respectively nearly the same as and slower than those for chron 2A, which are 0.394° Myr^{-1} and 0.622° Myr^{-1} when corrected to consistency with recent revisions to the timescale using the calibration factors given in DeMets *et al.* (1994b). Recalibrating to the timescale of Cande & Kent (1995) gives identical results. Thus the Indian plate has on average been rotating relative to the African plate at nearly the same rate since chron 2A (3 Ma) as since chron 5 (11 Ma). On the other hand, the Australian plate has on average been rotating relative to the African plate about 8 per cent faster since chron 2A (3 Ma) than the average since chron 5 (11 Ma). The chron 5 rotations can be transformed to average angular velocities by dividing the angle of each chron 5 rotation by the assumed age of the old end of

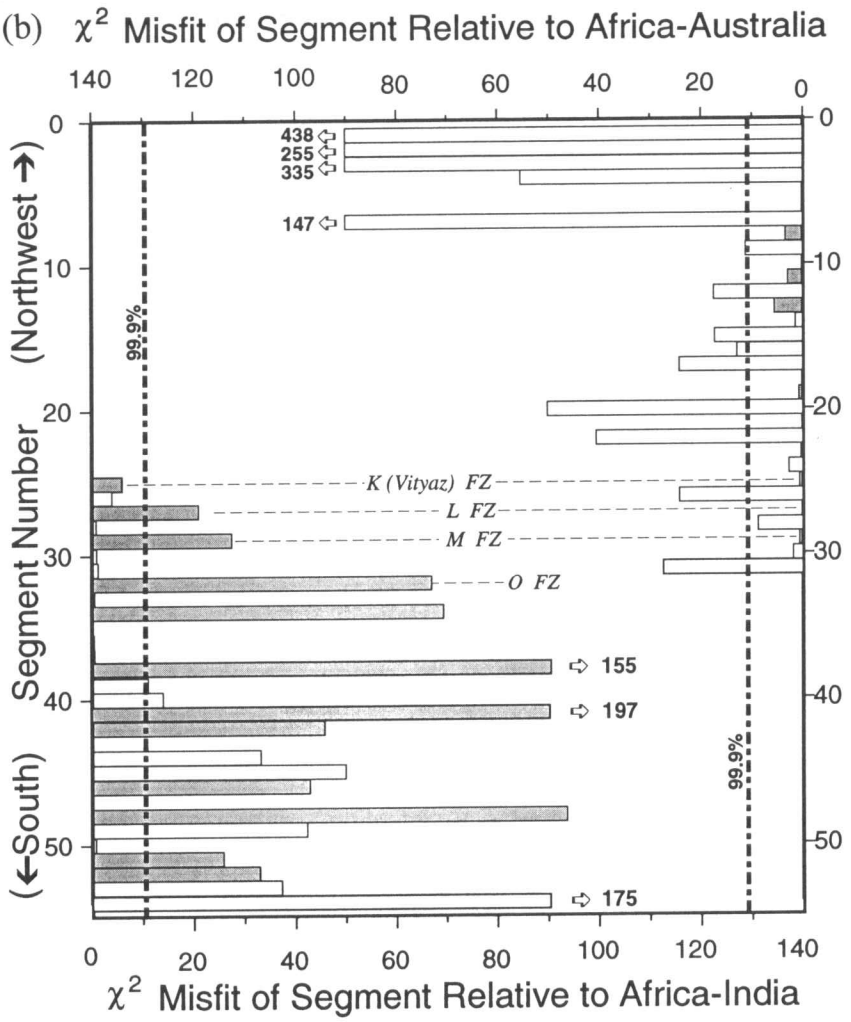

Figure 5. (*Continued.*)

chron 5 [10.949 Ma on the timescale of Cande & Kent (1995)]. The resulting angular velocity differs significantly from the average angular velocity since chron 2A (DeMets *et al.* 1994a) for both India relative to Africa (significance level of 0.04) and for Australia relative to Africa (significance level of 1×10^{-16}).

The major improvements in the determination of the Africa–India and Africa–Australia rotations give a much better determination of the India–Australia finite rotation (Table 3). The new India–Australia Euler pole is closer to the Chagos–Laccadive Ridge than is the pole of Royer & Chang (1991); the volume of the confidence region for the India–Australia rotation is reduced by a factor of 188 relative to the old. The new chron 5 Euler pole is close to the chron 2A pole of rotation (Fig. 6), suggesting that the India–Australia directions of motion have been stable since 11 Ma or the onset of motion, whichever is the more recent. The angular velocity estimated for India relative to Australia since 11 Ma differs insignificantly from that since 3 Ma.

DISCUSSION

Deformation of the African plate

An important assumption throughout our analysis is that the entire misfit can be attributed to motion between the Indian and Australian plates and that any deformation within the African plate is negligible for that portion of the plate flanking the Carlsberg and Central Indian ridges. There is, of course, significant deformation of the African plate across the East African Rift valleys and related extensional structures. It seems reasonable to speculate that some of this deformation might continue far enough eastwards to affect our analysis. We examine this assumption in light of the new results, three of which are particularly relevant. First, the fact that crossings from the Owen triple junction through spreading ridge corridor I–J are well fit shows that not only the Indian plate, but also the African plate, is rigid to an excellent degree of approximation where it flanks the Carlsberg Ridge and northernmost Central Indian Ridge. Second, the fact that crossings from the Rodrigues triple junction through fracture zone O are well fit shows that not only the Australian plate, but also the African plate, is rigid to an excellent degree of approximation where it flanks the central and southern Central Indian Ridge. If the African plate is deforming anywhere relevant to our study, it must therefore be between fracture zone O and fracture zone J. Fig. 9(a) shows the location of all off-ridge and off-transform fault earthquakes flanking this part of the Central Indian Ridge. None of the earthquakes, and for that matter no other independent indicator of deformation, lies on the

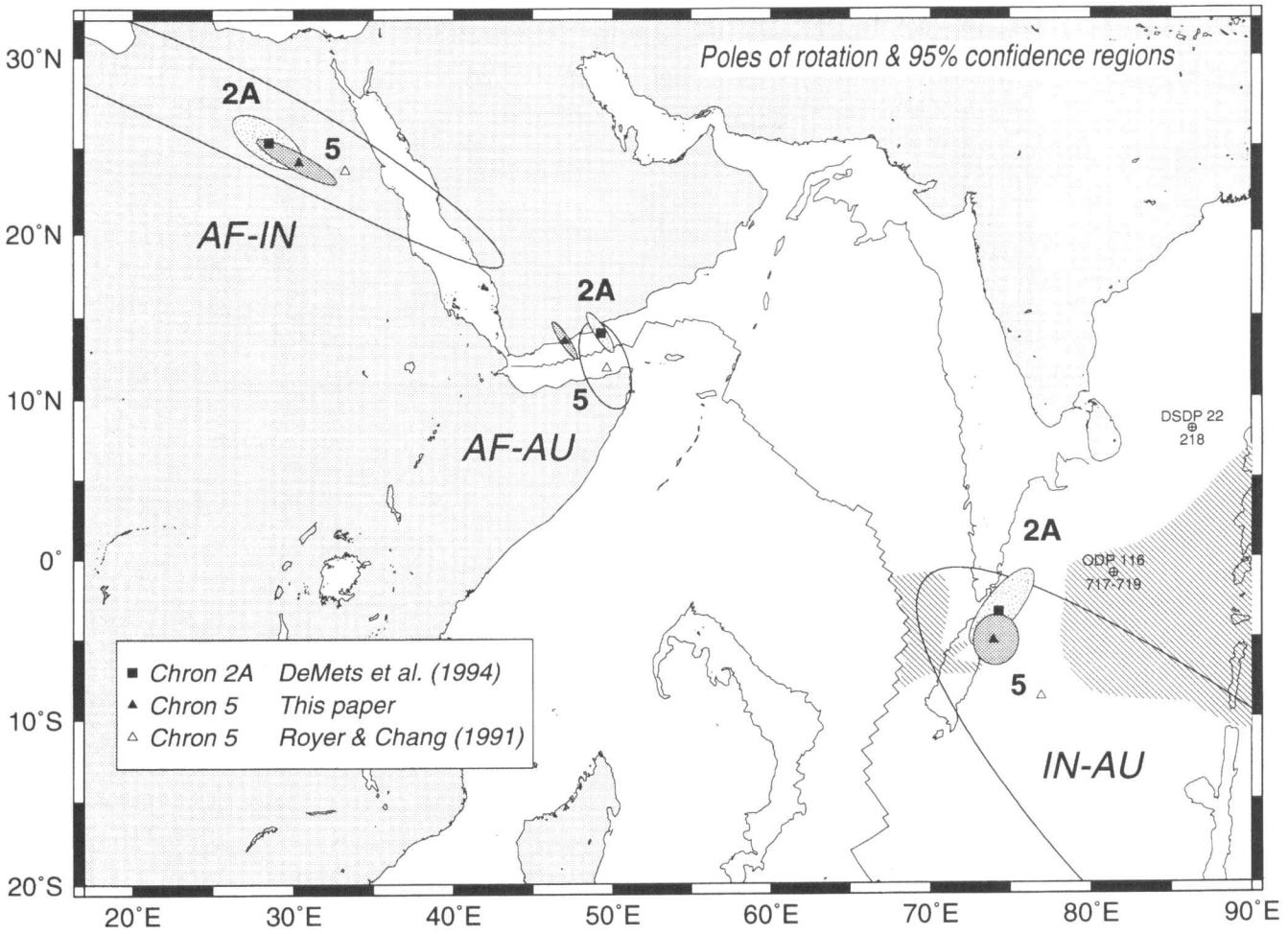

Figure 6. Location of the new chron 5 Euler poles and their 95 per cent confidence limits. The confidence regions are much smaller than those of Royer & Chang (1991), and are similar to the pole location for chron 2A (best-fitting poles from DeMets *et al.* 1994a). The two diagonally ruled regions show the approximate extent of the two disjointed zones of deformation that constitute the wide boundary between the Australian and Indian plates. The poles of rotation are in the apparently non-deforming zone between the two zones of deformation.

African side of the Central Indian Ridge. Third, when estimating the pole of rotation between India and Australia, we assume that Africa is rigid between fracture zones J and O. If Africa were deforming in this region, the estimated pole would differ from the true pole of rotation, which must lie between the western divergent and eastern convergent deforming zones that separate the Indian and Australian plates. The pole has compact confidence limits and lies neatly between the two deforming zones (Fig. 6). This good agreement indicates that the deformation, if any, within the part of the African plate flanking the Central Indian Ridge between fracture zones O and J is negligible.

Initiation of motion between India and Australia

Two unconformities can be traced from hills of folded sediments on the lower Bengal Fan and from the Ninetyeast Ridge through the conformable section between the hills throughout the Bay of Bengal (Curray & Moore 1971, 1974; Moore *et al.* 1974; Curray *et al.* 1982). The older unconformity, Eocene in age, occurs near Ninetyeast Ridge and in the Bay of Bengal but is unobserved south of 1°–2°N, where it appears to pinch out, presumably due to the lack of Eocene and older sedimentation farther south in the Bengal Fan (Curray & Munasinghe 1989). The younger of these two unconformities, thought by most workers to record the onset of deformation that is continuing today, was estimated from drilling at Deep Sea Drilling Program (DSDP) Site 218, which is near 8°N and about 500 km east of Sri Lanka and 400 km west of the Ninetyeast Ridge (Fig. 6), to be at latest Miocene in age (Moore *et al.* 1974). Curray, Moore, and colleagues hypothesized that this unconformity is regional and can be correlated over much of the northeastern Indian Ocean. For example, by tracing southwards and westwards from DSDP Site 218, Curray, Moore, and colleagues were able to show that growth structures off Sri Lanka started forming at the time of the late Miocene unconformity that was penetrated at Site 218 (Curray & Munasinghe 1989). Later drilling during Ocean Drilling Program (ODP) Leg 116 at about 1°S in the distal Bengal Fan about 800 km south of Sri Lanka dated an unconformity that marks the onset of the episode of deformation there that continues to the present. These later drill sites are about 1100 km southwest of DSDP Site 218 (Fig. 6). The unconformity was dated as 7.5–8.0 Ma (latest Miocene), which is consistent with the earlier hypothesis of a synchronous unconformity recording the onset of deformation over a huge

Table 3(a). Africa–India–Australia rotations.

Plate Pair	Latitude (°N)	Longitude (°E)	Angle (degrees)	χ^2	$\hat{\kappa}$	N	s	df
Africa-India	24.13	30.37	4.355±0.158	63.0	1.32	132	23	83
Africa-Australia	13.54	47.03	6.331±0.143	111.2	1.14	176	23	127
India-Australia	-5.17	73.94	2.626±0.268					

Rotations restore the first plate to its position with respect to the second plate. N is the number of anomaly and fracture-zone crossings, s is the number of great-circle segments, and df represents the degrees of freedom. Uncertainties following angles are 1-D 95 per cent confidence limits.

Table 3(b). Africa–India–Australia rotation covariances.

Plate Pair	a	b	c	d	e	f	g
Africa-India	0.670	1.323	-0.009	2.821	0.015	0.043	10^{-6}
Africa-Australia	0.419	0.835	-0.300	1.841	-0.635	0.243	10^{-6}
India-Australia	0.940	2.038	-0.194	4.856	-0.432	0.240	10^{-6}

Covariances are computed in a reference frame fixed to the first plate and thus describe uncertainties in the reconstructed location of the first plate for the rotations in (a). Covariance units are in units of radians^2 and have not been rescaled by the value of $\hat{\kappa}$.

The covariance matrix (without rescaling by $\hat{\kappa}$) can be constructed as follows:

$$\begin{pmatrix} a & b & c \\ b & d & e \\ c & e & f \end{pmatrix} \cdot g$$

Table 3(c). Africa–India–Australia covariance eigenvectors and eigenvalues.

Plate Pair	Eigenvalue$^{\frac{1}{2}}$ (degrees)	Eigenvector		Volume (degrees^3)	
		Lat. (°N)	Long. (°E)	This study	R&C 1991
Africa-India	0.0093	42.8	-25.6	5.64×10^{-5}	552×10^{-5}
	0.0136	47.2	154.7		
	0.1064	0.2	64.6		
Africa-Australia	0.0075	62.9	13.6	3.04×10^{-5}	238×10^{-5}
	0.0108	-19.9	-31.4		
	0.0897	-17.7	65.2		
India-Australia	0.0153	4.1	-22.7	22.7×10^{-5}	3100×10^{-5}
	0.0257	83.6	106.7		
	0.1376	-4.9	66.9		

Square roots of eigenvalues are 1-D, 1σ uncertainties and are derived from the covariances in (b). R&C 1991 indicates values from Royer & Chang (1991).

region (Ocean Drilling Program Leg 116 Shipboard Scientific Party 1987; Cochran 1990).

Our new results, combined with those of DeMets *et al.* (1994a), permit a simple-minded estimate of the age of onset of deformation in the Indian Ocean. Assuming an age of the reconstruction of 10.949 Ma gives an average rotation rate of $0.240 \pm 0.024°$ Myr^{-1}, which is insignificantly slower than the average rotation rate of $0.298 \pm 0.092°$ Myr^{-1} since 3 Ma (DeMets *et al.* 1994a,b) (these are both 95 per cent confidence limits). If we interpret these figures literally, a constant rate of rotation equal to the average rate since 3 Ma would imply that the India–Australia relative motions started at 8.8 ± 2.8 Ma (95 per cent confidence limits), which is not inconsistent with the age of the onset of deformation inferred from the drilling results. Caution is warranted in attaching any importance to this agreement, however, as the results of Royer & Chang (1991) suggest that motion between India and Australia began before chron 5 (11 Ma).

Some implications for the diffuse India–Australia plate boundary

The Australian plate has been rotating counterclockwise relative to the Indian plate about a pole located west of the Central Indian Basin, just east of the Chagos–Laccadive Ridge (Gordon *et al.* 1990; Royer & Chang 1991; DeMets *et al.* 1994a). Hence approximately north–south convergence increases with increasing distance eastwards from the pole of rotation in the Central Indian Basin; approximately north–south divergence increases with increasing distance west of the

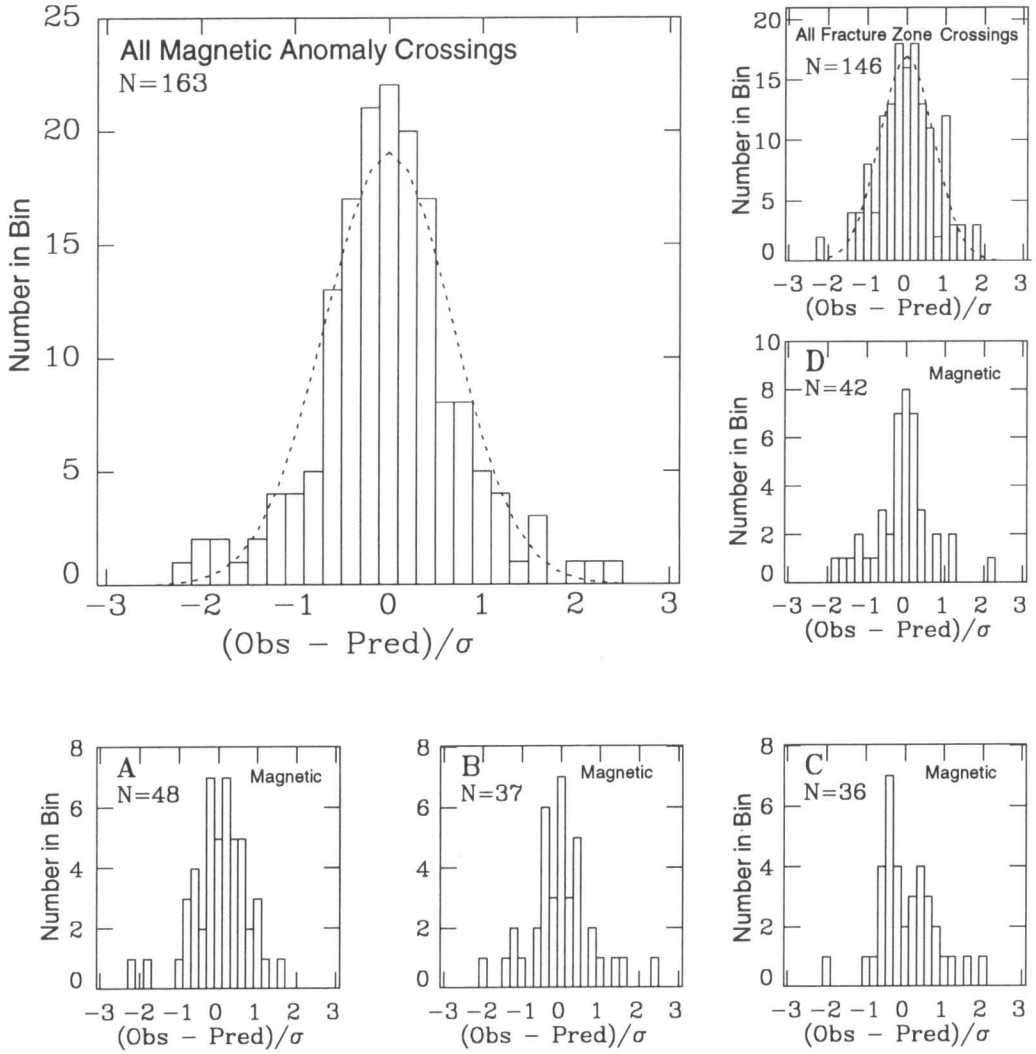

Figure 7. Histograms of data residuals: the horizontal axis shows the normalized residual distances between best-fitting great-circle segments and magnetic-anomaly and fracture-zone crossings. The residual distances are measured along a great circle orthogonal to the best-fitting great-circle segment and are divided by the estimated uncertainties for each point. The estimated uncertainties were determined through analysis of the dispersions of the fracture-zone crossings and subsets A to D of the magnetic-anomaly crossings; group A contains the highest-quality data, B the next highest, C the next, and D the lowest-quality data. The data used to construct the histograms consist of 141 magnetic-anomaly and fracture-zone crossings recording motion between Africa and India, and 173 magnetic-anomaly and fracture-zone crossings recording Africa–Australia motion. The dashed lines show the number of occurrences expected within bins with widths of 0.1 standard deviations for a normal error distribution with a mean of zero and standard deviation of 1.0. The total area beneath the curve equals N, the number of observations.

pole, i.e. between the Chagos–Laccadive ridge and the Central Indian Ridge. The stability of the India–Australia pole suggests that the same boundary conditions on deformation have prevailed since motion between India and Australia began or since 11 Ma, whichever is more recent. Furthermore, if motion started at or after 11 Ma we can quantify the components of the integral of deformation since chron 5 along paths through the diffuse plate boundary (Table 4). If motion began after 11 Ma, as many workers believe, then these estimates are integrals of the total deformation. For example, the north–south component of shortening along 80°E is 31 ± 7 km (1-D 95 per cent confidence limits) and along 90°E, 80 ± 12 km. If the diffuse boundary is ~900 km wide at 80°E [as indicated by seismic reflection profiling along 81.5°E (Chamot-Rooke *et al.* 1993)], the average north–south longitudinal strain is (3.4 ± 0.8) per cent (1-D 95 per cent confidence interval). If it is 2000 km wide at 90°E, the strain is (4.0 ± 0.4) per cent.

These estimates of shortening are larger than those from seismic profiles (Fig. 8). From migrated and depth-converted seismic sections, Bull & Scrutton (1992) estimated a total shortening of 18 ± 6 km between 80° and 82°E. From a longer (2100 km) north–south multichannel seismic line along 81.5°E (M/S Marion Dufresne MD70-1), horizontal throws could not be estimately directly. Instead, Chamot-Rooke *et al.* (1993) assumed a planar fault geometry and estimated the total shortening from vertical throws and from average dips of crustal faults. They identified 134 faults or folds in the sediments. Of these, 42 are associated with oblique crustal reflectors for which the apparent fault dip in the crust could be estimated. The average of all measured fault dips was used for the 92

Table 4(a). Component of length changes along great circles connecting points (in kilometers with 1-D 95 per cent confidence limits).

	Australian plate						
Indian plate	10°S 70°E	10°S 75°E	10°S 80°E	10°S 85°E	10°S 90°E	10°S 95°E	10°S 99°E
0°N 70°E	20 ± 4	6 ± 5	-4 ± 5	-11 ± 5	-15 ± 5	-18 ± 5	-19 ± 5
3°N 75°E	10 ± 3	-5 ± 4	-20 ± 5	-30 ± 6	-36 ± 6	-39 ± 6	-41 ± 6
3°N 80°E	1 ± 4	-14 ± 5	-31 ± 7	-44 ± 8	-50 ± 8	-53 ± 8	-54 ± 7
7°N 85°E	-1 ± 5	-17 ± 6	-36 ± 8	-55 ± 10	-71 ± 11	-80 ± 11	-83 ± 11
8°N 90°E	-5 ± 5	-20 ± 6	-38 ± 8	-60 ± 10	-80 ± 12	-95 ± 13	-102 ± 13

A negative value indicates shortening, whereas a positive value indicates stretching. Values were determined by reconstructing the points on the Australian plate relative to an arbitrarily fixed Indian plate and projecting the change in length and uncertainty region onto the original great circles in the fixed Indian plate reference frame.

Table 4(b). Percentage longitudinal strains along great circles connecting points (1-D 95 per cent confidence limits).

	Australian plate						
Indian plate	10°S 70°E	10°S 75°E	10°S 80°E	10°S 85°E	10°S 90°E	10°S 95°E	10°S 99°E
0°N 70°E	1.8 ± 0.3	0.5 ± 0.4	-0.3 ± 0.3	-0.5 ± 0.3	-0.6 ± 0.2	-0.6 ± 0.2	-0.6 ± 0.2
3°N75°E	0.6 ± 0.2	-0.4 ± 0.3	-1.3 ± 0.3	-1.6 ± 0.3	-1.6 ± 0.3	-1.5 ± 0.2	-1.3 ± 0.2
3°N 80°E	0.0 ± 0.2	-0.9 ± 0.3	-2.1 ± 0.5	-2.7 ± 0.5	-2.7 ± 0.4	-2.4 ± 0.3	-2.1 ± 0.3
7°N 85°E	0.0 ± 0.2	-0.8 ± 0.3	-1.8 ± 0.4	-2.9 ± 0.5	-3.5 ± 0.5	-3.5 ± 0.5	-3.3 ± 0.4
8°N 90°E	-0.2 ± 0.2	-0.8 ± 0.2	-1.7 ± 0.3	-2.8 ± 0.5	-3.9 ± 0.6	-4.4 ± 0.6	-4.4 ± 0.6

A negative value indicates shortening, whereas a positive value indicates stretching.

faults lacking directly measured dips. Apparent fault dips on the time sections were converted to dip by using a lower bound of 5 km s^{-1} and an upper bound of 7 km s^{-1} for the crustal velocity. These lower and upper velocity bounds give mean dips of 36° and 45°, respectively, and were used to obtain lower and upper limits on total shortening of 22 km and 37 km, corresponding to a longitudinal strain of 2.5–4.3 per cent. In comparison, the north–south component of shortening we calculate at 81.5°E is 38 ± 8 km, which is insignificantly larger than their estimate of shortening (Fig. 8).

Jestin (1994) estimated total shortening of 44 ± 10 km at 84.5°E on a 1000 km long line (MD70-2), which may not cross the entire deforming zone. This shortening is insignificantly smaller than the north–south component of shortening of 53 ± 9 km that our reconstructions indicate along 84.5°E. Jestin (1994) also reports a shortening of 15 ± 4 km from a single channel seismic profile (R/V Robert Conrad RC27-07) that apparently crosses the entire zone of deformed oceanic crust in the central Indian Ocean along 78.8°E. This estimate of shortening is marginally significantly less than the 24 ± 6 km of north–south shortening we calculate along 78.8°E. This estimate from the same seismic profile was later revised downwards, however, to 11.2 ± 2 km of shortening (Van Orman *et al.* 1995), which is significantly less than the shortening indicated by the plate reconstructions (Fig. 8).

Most of the differences are statistically insignificant and may simply reflect the combined uncertainties of the two sets of estimates. There are several possible explanations for the one significant difference, which may also contribute to the insignificant differences, including shallowing of faults with depth, underestimated shortening on many small faults not resolved by the seismic data, and displacements out of the vertical plane of the seismic profile. That the seismic profiles indicate consistently more convergence than that indicated since 3 Ma but consistently less convergence than that since 11 Ma suggests another possible explanation—that the seismic profiles only capture the deformation since 7.5–8.0 Ma whereas motion between India and Australia began before 7.5–8.0 Ma.

West of the Euler pole, north–south divergence of 20 ± 4 km occurs along 70°E (Table 4). According to our analysis, this north–south divergence should be accommodated mainly between fracture zone O, which is one fracture zone south of the Vema fracture zone, and fracture zone L, which is between the Vityaz and Vema fracture zones (Fig. 5). When the Indo-Australian crossings are rotated using the best-fitting Africa–Australia rotation, the magnetic anomaly crossings are systematically misfit at all spreading-ridge segments northwest of fracture zone O with even larger misfits northwest of fracture zone J (Fig. 9a). In contrast, when the Indo-Australian crossings are rotated using the Africa–India rotations, the misfit to fracture-zone crossings is apparent for fracture zones southeast of and including fracture zone L, and increases considerably for fracture zones southeast of and including the Vema (N) fracture zone, which suggests that the Vema fracture zone may have been the locus of considerable deformation (Fig. 9b). That the trace of the Vema fracture zone mapped by the satellite-derived gravity appears less continuous on the Indo-Australia side of the Central Indian Ridge than on the African

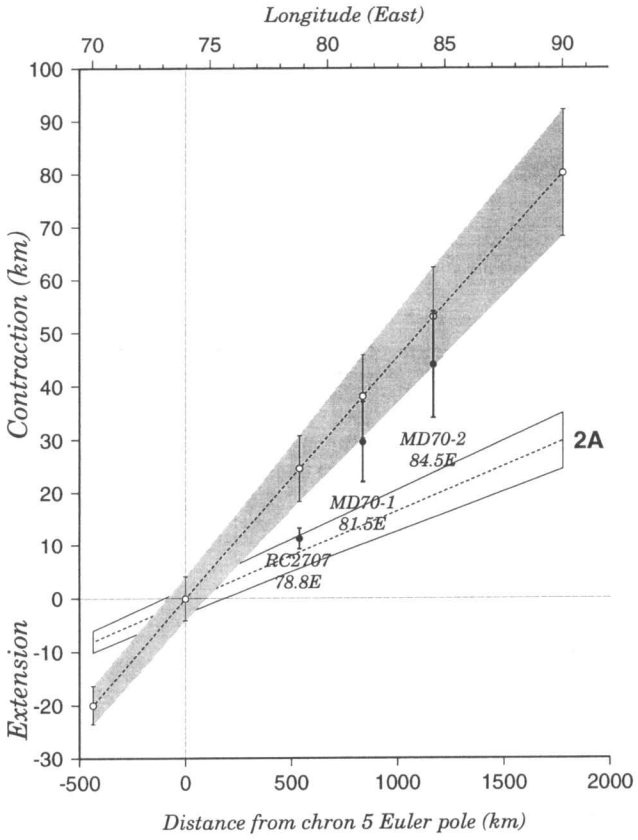

Figure 8. Predicted north–south component of relative motion between India and Australia east (contraction) and west (extension) of the chron 5 Euler pole with 95 per cent confidence limits (stippled area). Solid circles and error bars (95 per cent confidence limits) show the amount of north–south shortening measured from seismic profiles in the central Indian Basin (Chamot-Rooke *et al.* 1993; Jestin 1994; Van Orman *et al.* 1995). Also shown are the north–south components (and 95 per cent confidence limits) of motion between India and Australia since chron 2A (3 Ma) (DeMets *et al.* 1994a).

side is also consistent with its having been the locus of considerable deformation.

A rotation of the Indian plate relative to an arbitrarily fixed Australian plate about the chron 5 India–Australia Euler pole mainly affects the fit to the magnetic crossings; this effect becomes more important for the lineations located above (i.e. northwest of) the Euler pole in Fig. 9(a). A rotation of the Australian plate relative to an arbitrarily fixed Indian plate about the chron 5 India–Australia Euler pole mainly affects the fit to the fracture zones; this effect becomes important for the fracture zones located to the left of the Euler pole in Fig. 9(b). This qualitative analysis illustrates what the statistical tests are indicating.

Earthquakes (Fig. 9, also see Fig. 20 from DeMets *et al.* 1994a) west of the India–Australia Euler pole can be divided into two groups: a cluster of earthquakes with east–west-striking normal fault mechanisms located on the Chagos Bank and a disseminated group of earthquakes with strike-slip mechanisms consistent with right-lateral slip on southwest–northeast vertical planes parallel to, or coinciding with, the fracture zones. The first group clusters on grabens that are visible on the satellite-derived gravity data (Fig. 3a), whereas the strike-slip mechanisms roughly span the same area as the deformed zone inferred from plate reconstructions. Some off-ridge events occur northwest of fracture zone L, however, indicating that the deformation continues farther northwest than can be demonstrated from the plate-motion data. This pattern suggests that southwest of the India–Australia Euler pole, the divergence is accommodated mainly by normal faulting near the Chagos Bank and that farther west the extension is distributed, with slip mainly occurring on re-activated fracture zones. The strike-slip mechanisms can accommodate north–south divergence if the fracture zones and the blocks of seafloor between them are rotating counterclockwise.

Increase in deformation as a function of distance from the Euler pole

That the shortening estimated from the seismic profiles increases eastwards away from the pole of rotation between 78.8°E and 84.5°E (Fig. 8) has been emphasized by Van Orman *et al.* (1995). Although we are sceptical of the accuracy of estimates of shortening from seismic profiles, we are encouraged by the eastward increase in the north–south component of shortening inferred from the profiles (Fig. 8). In our view, these profiles, which span about a 600 km range of distance from the pole of rotation, are a small sample of a much larger pattern evident from other data. Over a larger region, the existence of a pronounced gradient from west to east in the north–south integral of north–south deformation is shown by several independent indicators of deformation. In the western deforming zone, the deformation clearly indicates north–south stretching of the Indo-Australian oceanic lithosphere. All evidence for this stretching vanishes once the Chagos trough is crossed eastwards. There is then a range of longitudes from about 74°E to about 77°E for which there is no evidence for deformation (Figs 6 and 9a), including an absence of earthquakes detectable with ocean-bottom seismometers (Levchenko & Ostrovsky 1992). Subtle indications in the satellite-derived gravity of the east–west-striking undulations interpreted as indicating north–south shortening occur from about 77°E to 80°E (Fig. 3a). East of 80°E, the gravity and geoid undulations are more obvious and moderate to large earthquakes occur. This gradient in deformation, from north–south stretching in the west, through an absence of deformation from ~74°E to ~77°E, and continuing from subtle to obvious evidence of north–south contraction farther east, is manifested over thousands of kilometres and is documented by many independent types of observations: locations and focal mechanisms of earthquakes, topographic expressions of both north–south stretching (e.g. the grabens adjacent to Chagos Bank) and north–south contraction (i.e. the east–west-striking topographic and geoidal undulations), and the thrust faulting and folding revealed by seismic reflection profiles.

CONCLUSIONS

The increase in number and quality of the data have led to the following new results.

(1) The new altimetry data has permitted the delineation of all the fracture zones, as well as some wandering offsets and other fine-scale features. There are 32 palaeotransform faults and five non-transform offsets that appear to be wandering

(a)

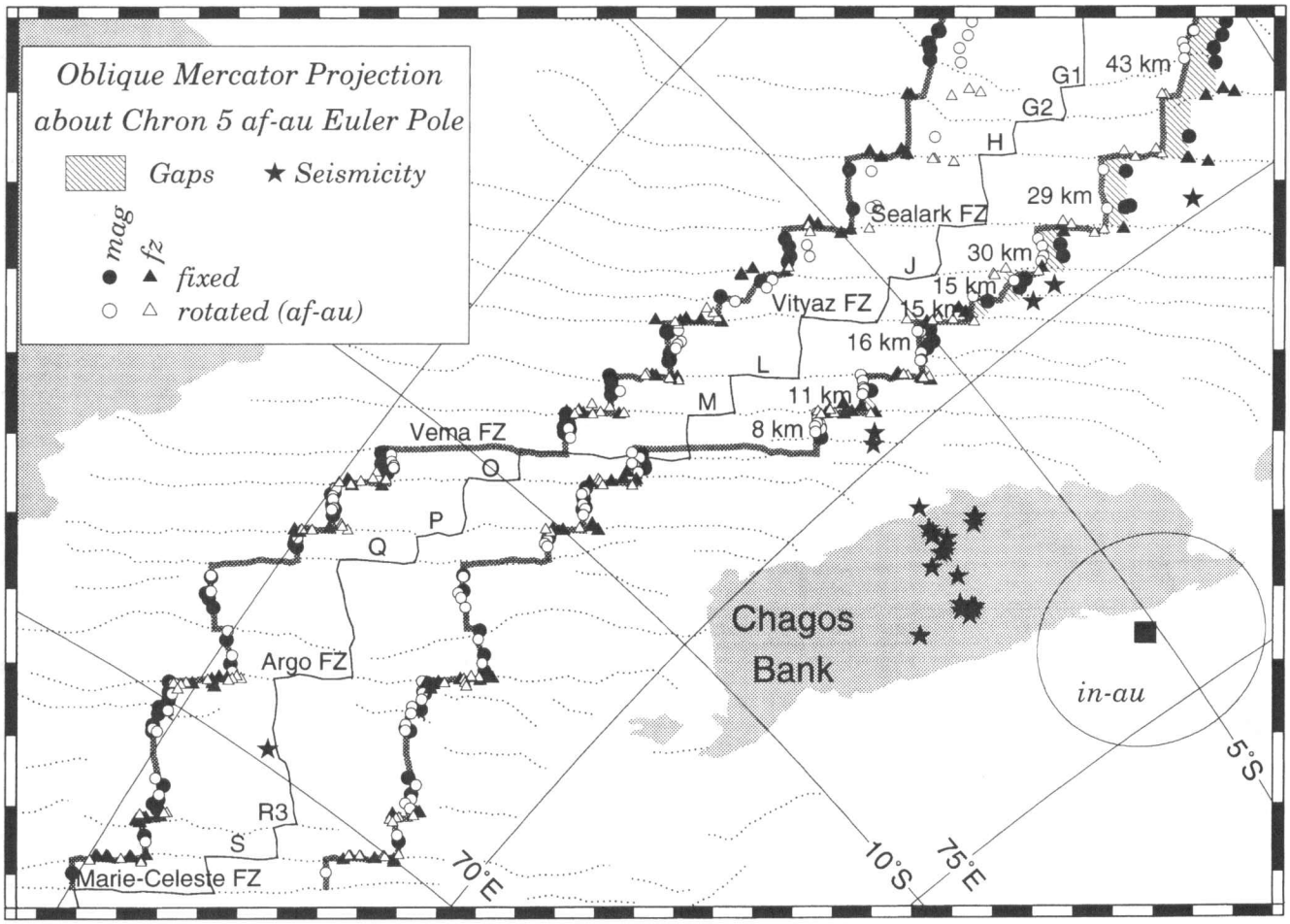

Figure 9. Chron 5 reconstructions in the vicinity of the Africa–Australia–India triple junction in oblique Mercator projections about (a) the Africa–Australia and (b) Africa–India chron 5 Euler poles (frame alternates colour at intervals of 1° in the oblique Mercator coordinate system). Solid symbols show the locations of magnetic-anomaly or fracture-zone crossings, whereas empty symbols show the same crossings rotated by the chron 5 rotation, that for Africa to Australia or vice versa for part (a) and that for Africa to India or vice versa for part (b). The continuous thick line is an estimate of isochron 5 on the African plate, which is presumably little deformed or undeformed. It is also shown rotated onto the Indo-Australian side of the Carlsberg Ridge and Central Indian Ridge. The resulting large gaps between the rotated isochron and observed isochron on the Indo-Australian side are shown by diagonally ruled regions. The Africa–Australia rotation (part a) mainly mismatches the magnetic-anomaly crossings, from the ridge segment immediately north of fracture zone O and northwards. The Africa–India rotation (part b) mainly mismatches the fracture zones south of fracture zone L and southwards.

offsets along the Central Indian and Carlsberg ridges. The mean distance between palaeotransform faults along the Carlsberg Ridge is 200 km; the median distance is poorly defined, being between 101 and 195 km. The mean distance between fracture zones along the Central Indian Ridge is 96 km; the median is 59 km.

(2) The analysis of dispersion of magnetic-anomaly and fracture-zone crossings shows that the uncertainties are smaller than assumed in prior work. The dispersion of the crossing locations about the best-fitting models indicates that the 1-D 1σ uncertainties are on average 3 to 5 km for the magnetic anomaly crossings and about 4 km for the fracture-zone crossings.

(3) Analyses of magnetic anomaly 5 and corresponding fracture-zone data indicate that, when the Africa–Australia data are fit optimally, gaps as large as 90–100 km occur between the African and the Indian magnetic-anomaly crossings. Conversely, when the Africa–India data are fit optimally, a combined gap as large as about 90 km occurs between the African and the Australian fracture-zone and magnetic-anomaly crossings (Fig. 4).

(4) With the new data along the Central Indian Ridge, the chron 5 Australia–Africa rotation can now be usefully and accurately estimated directly, i.e. without using plate-motion data along the Southwest Indian Ridge and Southeast Indian Ridge, as was required in prior work.

(5) The new confidence regions on the rotations are much smaller than found before; the volumes of the confidence regions are 98, 78, and 188 times smaller, respectively, for Africa–India, Africa–Australia, and Australia–India than found before. The rotations of Royer & Chang (1991) lie outside the confidence regions of the newly determined rotations, reflecting the much smaller confidence regions found in our study. The new small-confidence regions permit very specific predictions to be made about where north–south divergence has been occurring, where north–south convergence has been occurring,

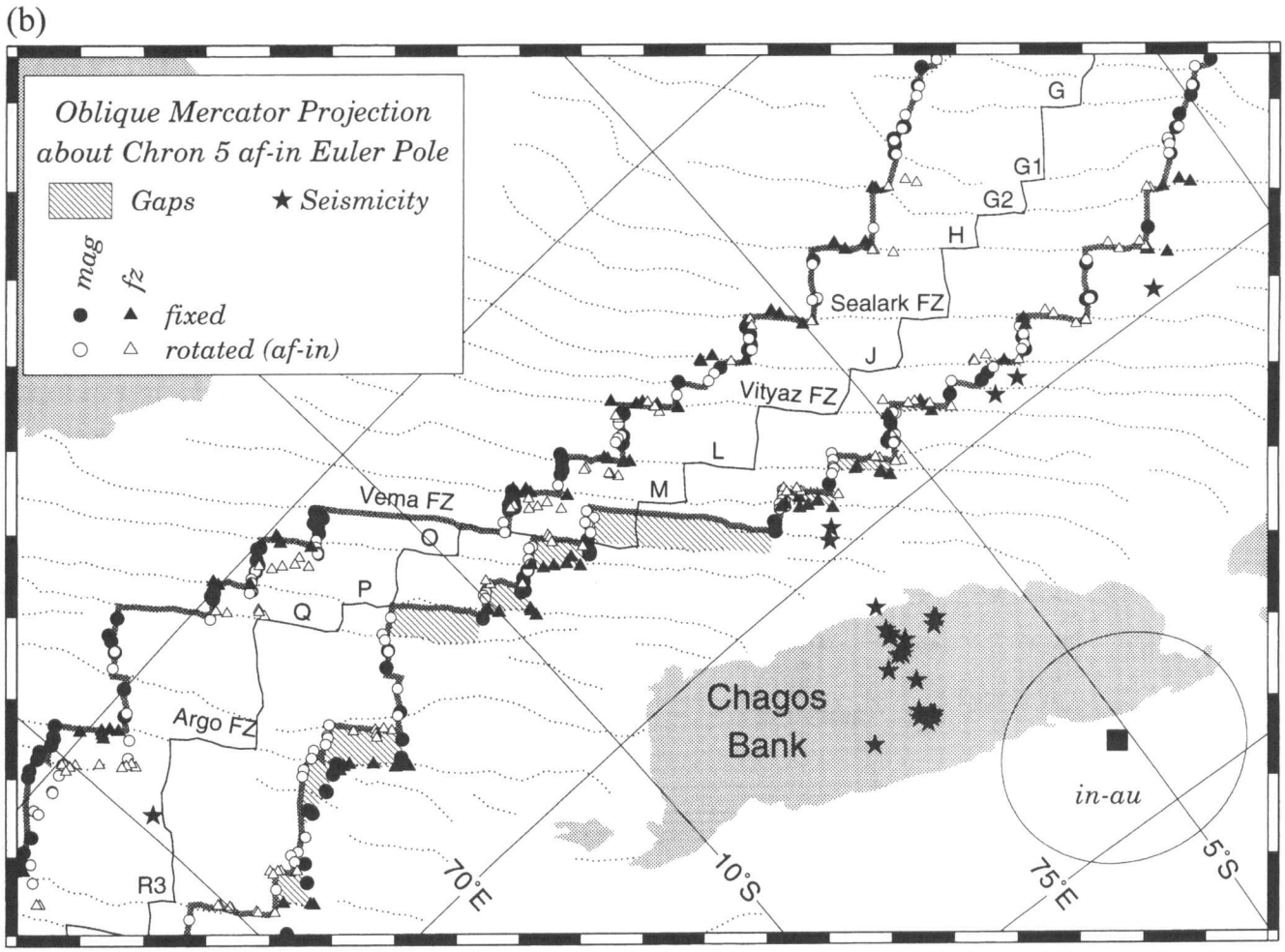

Figure 9. (*Continued.*)

and where the deformation rate is expected to be small (i.e. near the pole of rotation, which has compact confidence limits). The motion accommodated across the diffuse plate boundary near the pole of rotation has been negligible, with net convergence increasing eastwards and net divergence increasing westwards from the pole of rotation. These qualitative predictions are consistent with a large body of independent data that record past and present deformation in the diffuse plate boundary zone.

(6) The chron 2A poles of rotation are similar to the chron 5 poles of rotation for both Africa–India and Africa–Australia motion. The difference is insignificant in the former case but significant in the latter case, for which the chron 2A pole lies east of the chron 5 pole. The average angular velocity of Australia relative to Africa differs at the 1.4×10^{-16} level and indicates that the 3-Myr-average motion is both more easterly and slightly faster than the 11-Myr-average motion. The average angular velocity of India relative to Africa since chron 2A (3 Ma) has been nearly the same as that since chron 5 (11 Ma); these two average angular velocities differ at the 4 per cent significance level.

(7) The pole of rotation between India and Australia since chron 5 is located at 5°S, 74°E, near the eastern edge of the Chagos–Laccadive Ridge. It differs insignificantly from the pole of rotation over the past 3 Myr (i.e. since chron 2A), which is located at 3°S, 74°E. The average angular velocity since chron 2A (3 Ma) also differs insignificantly from that since chron 5 (11 Ma). This similarity suggests that information about motion and deformation at present, since 3 Ma, and since 11 Ma can be combined to obtain a more comprehensive kinematic model for how the relative motion between the Indian and Australian plates is and has been accommodated in the diffuse plate boundary.

(8) The resolution along the Central Indian Ridge of where distributed deformation has occurred within the wide India–Australia plate boundary is now much improved with the prior data gap of more than 2000 km now being well filled (Fig. 1). These data show the location of the intersection of the boundary between the Indian and Australian plates with the Central Indian Ridge and demonstrate that the boundary is at least a few hundred kilometres wide (i.e. from and including fracture zone L southwards to, but excluding, fracture zone O) at this intersection.

(9) Specific and accurate estimates of the integral of deformation along paths through the wide Australia–India plate boundary can now be made. The rotation since chron 5 has been used to determine specific quantitative estimates of the integral of deformation on north–south paths through the diffuse plate boundary. Near the Central Indian Ridge, along a meridian at 70°E, the diffuse plate boundary has accom-

modated 20 ± 4 km (1-D 95 per cent confidence limits) of north–south divergence since 11 Ma (chron 5). East of the pole of rotation, in the Central Indian Basin, the integral of shortening along meridians at 80°E and 90°E is 31 ± 7 km and 80 ± 12 km (1-D 95 per cent confidence limits), respectively.

(10) Insofar as the quoted uncertainties on shortening estimated from seismic profiles are valid, the shortening estimated from seismic profiles along 81.5°E and 84.5°E is significantly greater than the convergence since 3 Ma (i.e. chron 2A), whereas the shortening estimated from seismic profiles along 78.8°E is insignificantly greater than that since 3 Ma. The north–south shortening estimated along 81.5°E and 84.5°E from seismic profiles is insignificantly less than the shortening indicated from the plate reconstructions since 11 Ma (i.e. chron 5), but the seismic estimate of north–south shortening along 78.8°E is significantly less than indicated by the plate reconstructions. The discrepancy with the chron 5 reconstructions has several possible explanations including shallowing of faults with depth, underestimated shortening on many small faults not resolved by the seismic data, displacements out of the vertical plane of the seismic profile, or that the 7.5–8.0 of deformation estimated from the seismic profiles is less than the total deformation, as would be the case if motion started before 7.5–8.0 Ma.

(11) Although the data suggest a small acceleration in the motion of India relative to Australia between chrons 5 and 2A (11 and 3 Ma), it is impossible to determine from the plate-reconstruction data in hand whether the motion between the Indian and Australian plates began before chron 5, as Royer & Chang (1991) suggested, or since chron 5, in particular at 7.5–8.0 Ma as indicated by the DSDP and ODP drilling results (Moore *et al.* 1974; Ocean Drilling Program Leg 116 Shipboard Party 1987). Answering this question will require a comparison of motion between India and Australia since chron 5, with motion inferred from reconstructions for other ages (e.g. chron 6, 20 Ma).

ACKNOWLEDGMENTS

We thank David Sandwell for providing the stacked altimeter profiles, and the European Space Agency for access to the ERS-1 data. This work was supported by the Centre National de la Recherche Scientifique (CNRS) and Plan National de Télédétection Spatiale (J-YR), the NSF/CNRS cooperative program (J-YR, RGG, CD; NSF grant INT-9314549), and NSF grants OCE-9218541, OCE-9596284, and OCE-9417461 (RGG, CD). This work began when RGG was on sabbatical in Villefranche-sur-mer with support from CNRS, NSF, and Northwestern University. Most of the figures were drafted using the GMT software (Wessel & Smith 1991). CNRS Géosciences Azur contribution number 91.

REFERENCES

Atwater, T., 1989. Plate tectonic history of the northeast Pacific and western North America, in *Decade of North American Geology, The Geology of North America N: The Eastern Pacific Region,* pp. 21–72, eds Winterer, E.L., Hussong, D.M. & Decker, R.W., Geological Society of America, Boulder, CA.

Bull, J.M., 1990. Structural style of intra-plate deformation, Central Indian Ocean Basin: evidence for the role of fracture zones, *Tectonophysics,* **184,** 213–228.

Bull, J.M. & Scrutton, R.A., 1990. Fault reactivation in the central Indian Ocean and the rheology of oceanic lithosphere, *Nature,* **344,** 855–858.

Bull, J.M. & Scrutton, R.A., 1992. Seismic reflection images of intraplate deformation, Central Indian Ocean, and their tectonic significance, *J. Geol. Soc. Lond.,* A, **149,** 955–966.

Cande, S.C. & Kent, D.V., 1995. Revised calibration of the geomagnetic polarity timescale for the Late Cretaceous and Cenozoic, *J. geophys. Res.,* **100,** 6093–6095.

Chamot-Rooke, N., Jestin, F., de Voogd, B. & Phèdre Working Group, 1993. Intraplate shortening in the central Indian Ocean determined from a 2100-km-long north–south deep seismic reflection profile, *Geology,* **21,** 1043–1046.

Chang, T., 1987. On the statistical properties of estimated rotations, *J. geophys. Res.,* **87,** 6319–6329.

Chang, T., 1988. Estimating the relative rotation of two tectonic plates from boundary crossings, *J. Am. Stat. Assoc.,* **83,** 1178–1183.

Chaubey, A.K., Krishna, K.S., Subba Raju, L.V. & Gopala Rao, D., 1990. Magnetic anomalies across the southern Central Indian Ridge: Evidence for a new transform fault, *Deep-Sea Research,* **37,** 647–656.

Chaubey, A.K., Bhattacharya, G.C., Murty, G.P.S. & Desa, M., 1993. Spreading history of the Arabian Sea: Some new constraints, *Marine Geology,* **112,** 343–352.

Cochran, J.R., 1990. Himalayan uplift, sea level, and the record of Bengal Fan sedimentation at the ODP leg 116 sites, in *Proc. Ocean Drilling Program, Scientific Results,* **116,** pp. 397–414, eds Cochran, J.R., Stow, D.A.V., *et al.,* Ocean Drilling Program, College Station, Texas.

Curray, J.R. & Moore, D.G., 1971. Growth of the Bengal Deep-Sea Fan and denudation in the Himalayas, *Geol. Soc. Am. Bull.,* **82,** 563–572.

Curray, J.R. & Moore, D.G., 1974. Sedimentary and tectonic processes in the Bengal deep-sea fan and geosyncline, in *Geology of Continental Margins,* pp. 617–627, eds Burk, C.A. & Drake, C.L., Springer Verlag, New York, NY.

Curray, J.R. & Munasinghe, T., 1989. Timing of intraplate deformation, northeastern Indian Ocean, *Earth planet. Sci. Lett.,* **94,** 71–77.

Curray, J.R., Emmel, F.J., Moore, D.G. & Russel, W.R., 1982. Structure, tectonics, and geological history of the northeastern Indian Ocean, in *The Ocean Basins and Margins,* vol. 6, *The Indian Ocean,* eds Nairn, A.E. & Stheli, F.G., pp. 399–450, Plenum Press, New York, NY.

DeMets, C., Gordon, R.G. & Argus, D.F., 1988. Intraplate deformation and closure of the Australia–Antarctica–Africa plate circuit, *J. geophys. Res.,* **93,** 11 877–11 897.

DeMets, C., Gordon, R.G. & Vogt, P., 1994a. Location of the Africa–Australia–India triple junction and motion between the Australian and Indian plates: Results from an aeromagnetic investigation of the Central Indian and Carlsberg ridges, *Geophys. J. Int.,* **119,** 893–930.

DeMets, C., Gordon, R.G., Argus, D.F. & Stein, S., 1994b. Effect of recent revisions to the geomagnetic reversal timescale on estimates of current plate motion, *Geophys. Res. Lett.,* **21,** 2191–2194.

Dyment, J., 1991. Structure et évolution de la lithosphère océanique dans l'océan Indien: apport des anomalies magnétiques, *Thèse de Doctorat,* Université de Strasbourg, Strasbourg.

Eittreim, S. & Ewing, J., 1972. Mid-plate tectonics in the Indian Ocean, *J. geophys. Res.,* **77,** 6413–6421, 1972.

Engel, C.G. & Fisher, R.L., 1975. Granitic to ultramafic rock complexes of the Indian Ocean ridge system, western Indian Ocean, *Geol. Soc. Am. Bull.,* **86,** 1553–1578.

Fisher, R.L., Sclater, J.G. & McKenzie, D.P., 1971. Evolution of the central Indian Ridge, western Indian Ocean, *Geol. Soc. Am. Bull.,* **82,** 553–562.

Fisher, R.L., Jantsch, M.Z. & Comer, R.L., 1982. *General Bathymetric Chart of the Oceans (GEBCO), Sheet 5.09,* Canadian Hydrographic Service, Ottawa.

Glebovsky, V.Y. *et al.,* 1995. Mid-ocean ridges and deep oceanic basins: AMF structure, in *Anomalous Magnetic Field of the World Ocean,* ed. Gorodnitsky, A.M., CRC Press, Boca Raton.

Gordon, R.G. & DeMets, C., 1989. Present-day motion along the Owen Fracture Zone and Dalrymple Trough in the Arabian Sea, *J. geophys. Res.,* **94,** 5560–5570.

Gordon, R.G., Stein, S., DeMets, C. & Argus, D.F., 1987. Statistical tests for closure of plate motion circuits, *Geophys. Res. Lett.,* **14,** 587–590.

Gordon, R.G., DeMets, C. & Argus, D.F., 1990. Kinematic constraints on distributed lithospheric deformation in the equatorial Indian Ocean from present motion between the Australian and Indian plates, *Tectonics,* **9,** 409–422.

Hellinger, S.J., 1981. The uncertainties of finite rotations in plate tectonics, *J. geophys. Res.,* **86,** 9312–9318.

Jestin, F., 1994. Cinématique rigide et déformations dans la jonction triple Afar et dans le basin Indien Central, *Thèse de Doctorat,* University Pierre et Marie Curie, Paris.

Karasik, A.M., Mercuriev, S.A., Mitin, L.I., Sochevanova, N.A. & Yanovsky, V.N., 1986. Peculiarities in the history of opening of the Arabian Sea from systematic magnetic survey data, *Documents of the Academy of Sciences of USSR,* **286,** 933–938.

Levchenko, O.V. & Ostrovsky, A.A., 1992. Seismic seafloor observations: a study of 'anomalous' intraplate seismicity in the north-eastern Indian Ocean, *Phys. Earth planet. Inter.,* **74,** 173–182.

McAdoo, D.C. & Sandwell, D.T., 1985. Folding of oceanic lithosphere, *J. geophys. Res.,* **90,** 8563–8569.

Minster, J.B. & Jordan, T.H., 1978. Present-day plate motions, *J. geophys. Res.,* **83,** 5331–5354.

Molnar, P. & Stock, J.M., 1985. A method for bounding uncertainties in combined plate reconstructions, *J. geophys. Res.,* **90,** 12 537–12 544.

Molnar, P., Pardo-Casas, F. & Stock, J., 1988. The Cenozoic and Late Cretaceous evolution of the Indian Ocean Basin: uncertainties in the reconstructed positions of the Indian, African and Antarctic plates, *Basin Research,* **1,** 23–40.

Moore, D.G., Curray, J.R., Raitt, R.W. & Emmel, F.J., 1974. Stratigraphic-seismic section correlations and implications to Bengal Fan history, *Initial Rep. Deep Sea Drill. Proj.,* **22,** 403–412.

Müller, R.D. & Roest, W.R., 1992. Fracture zones in the North Atlantic from combined Geosat and Seasat data, *J. geophys. Res.,* **97,** 3337–3350.

Müller, R.D., Sandwell, D.T., Tucholke, B.E., Sclater, J.G. & Shaw, P.R., 1991. Depth to basement and geoid expression of the Kane fracture zone: A comparison, *Marine geophys. Res.,* **13,** 105–129.

Ocean Drilling Program Leg 116 Shipboard Scientific Party, 1987. Collisions in the Indian Ocean, *Nature,* **330,** 519–521.

Patriat, P., 1987. *Reconstitution de l'évolution du système de dorsales de l'océan Indien par les méthodes de la cinématique des plaques,* Publ. Territoire des Terres Australes et Antarctiques Françaises, Paris.

Royer, J.-Y. & Chang, T., 1991. Evidence for relative motions between the Indian and Australian plates during the last 20 Myr from plate tectonic reconstructions. Implications for the deformation of the Indo-Australian plate, *J. geophys. Res.,* **96,** 11 779–11 802.

Sandwell, D.T., 1984. A detailed view of the south Pacific geoid from satellite altimetry, *J. geophys. Res.,* **89,** 1089–1104.

Smith, W.H.F. & Sandwell, D.T., 1995. Marine gravity field from declassified Geosat and ERS-1 altimetry (abstract), *EOS, Trans. Am. geophys. Un.,* **76** *(Suppl.),* F156.

Stein, S. & Okal, E.A., 1978. Seismicity and tectonics of the Ninetyeast Ridge area: Evidence for internal deformation of the Indian plate, *J. geophys. Res.,* **83,** 2233–2245.

Stock, J.M. & Molnar, P., 1983. Some geometrical aspects of uncertainties in combined plate reconstructions, *Geology,* **11,** 697–701.

Stock, J. & Molnar, P., 1988. Uncertainties and implications of the Late Cretaceous and Tertiary position of North America relative to the Farallon, Kula, and Pacific plates, *Tectonics,* **7,** 1339–1384.

Sykes, L.R., 1970. Seismicity of the Indian Ocean and a possible nascent island arc between Ceylon and Australia, *J. geophys. Res.,* **75,** 5041–5055.

Tisseau, J., 1978. Etude structurale du Golfe d'Aden et du bassin de Somalie (Océan Indien occidental nord), *Thèse de 3ème cycle,* Université Paris-Sud, Paris.

Van Orman, J., Cochran, J.R., Weissel, J.K. & Jestin, F., 1995. Distribution of shortening between the Indian and Australian plates in the central Indian Ocean, *Earth planet. Sci. Lett.,* **133,** 35–46.

Weissel, J.K., Anderson, R.N. & Geller, C.A., 1980. Deformation of the Indo-Australian plate, *Nature,* **287,** 284–291.

Wessel, P. & Smith, W.H.F., 1991. Free software helps map and display data, *EOS, Trans. Am. geophys. Un.,* **72,** 441–445.

Wiens, D.A. *et al.,* 1985. A diffuse plate boundary model for Indian Ocean tectonics, *Geophys. Res. Lett.,* **12,** 429–432.

Yale, M.M., Sandwell, D.T. & Smith, W.H.F., 1995. Comparison of along-track resolution of stacked Geosat, ERS 1, and TOPEX satellite altimeters, *J. geophys. Res.,* **100,** 15 117–15 127.